

Reviewer #1

In this manuscript, the authors applied an energy balance model, SEBS, which was developed by the authors group before, to evaluate whole China's terrestrial surface energy balances in 0.1-degree spatial resolution by making the maximum use of satellite data sets. The results show that the estimated fluxes are well represented in China. Comparisons with the eddy covariance measurements and other data sets show that the energy and radiation fluxes by the proposed approach attained one of the best performances among the data sets.

Generally, the global surface energy flux data sets, including reanalysis data, do not have enough spatial and temporal resolution when looking at the national-level fluxes. The surface flux data sets from reanalysis data sets still contain large uncertainty. Therefore, this reviewer agrees with the authors that it is necessary to produce spatially and temporal higher resolution surface flux data sets.

RESPONSE: *We thank the reviewer for these appreciated comments. We fully agree with them. We have added more detailed discussions as the reviewers has pointed out. To give the readers a fully understanding of our work, the following paragraph was added in the new manuscript,*

'Generally, the global surface energy flux data sets, including reanalysis data, do not have enough spatial and temporal resolution when looking at the national-level fluxes. The surface flux data sets from reanalysis data sets still contain large uncertainty, partly due to the deficiency in their land surface process models that simulate land surface temperature by solving soil thermal transport equations (Chen et al., 1996) and usually result in a large error in LST simulation (Chen et al., 2011; Wang et al., 2014) if the model is not properly calibrated by measurements (Hogue et al., 2005). So the hypothesis tested in this paper is if it is possible to overcome the complex process in the soil by using satellite observed land surface temperature directly to calculate the land surface fluxes at continental scale? This study has demonstrated a benchmark on how to use satellite to derive a land surface flux dataset for a continental area on a personal laptop which is absolutely not feasible for the land surface process modeler to do in such a time and resource economic way.' on page 25.

My major concerns are below: 1. From the current manuscript, it is not easy to find the novelty of this study. I understand that energy and radiation fluxes estimation across China in such a high spatial resolution is new. But I feel this may not be enough because the suits of equations used in this approach were developed in the past studies (Su et al., 2002) and there are other energy flux estimation studies with satellite data sets as is cited in this manuscript. It may be necessary to make an introduction to let readers know where is the novelty of this study.

Response: *Actually, part of the innovative points have been explained in introduction, model development, input dataset preparation, and dealing with a large heterogeneous data. We agree that the basic equations were developed in the past studies. However the past studies do not give solutions on how to upscale the model to a continental area. The meteorological forcing data and satellite product used in our work are also from other studies. But the problems is why we chose these dataset but not others? and how to*

combine several sources of dataset and use them in our study? Is the dataset applicable or not? All these issues need to be tackled before the model run. These experience and accumulated knowledge have never been reported in other papers. Thus firstly, we have innovated ways of using the model.

Secondly, and certainly, the flux product is also one novelty of this work (on page 14491, line 24-26). As scientists have pointed out a spatially and temporally estimate of surface energy fluxes is urgently need by hydrological and meteorological studies due to that ‘all the available flux datasets are based on model simulations, which have deficiencies for studying changes in water-cycle and land–air interactions in China’. As you have seen in our response to your previous comment that we also added another paragraph to make the second novelty to be clearer to the reader.

Thirdly, there are so many challenges in the beginning of the work, such as: difficulties in producing an accurate estimate of water and energy spatial distribution at a continental scale with remote sensing method. Remote sensing approaches to estimate surface heat and water fluxes have been largely used on regional scales, but there is rarely satellite-derived data which could be used for land-atmosphere interaction studies for continental area (on page 14474, line19-24). But here, we have made the first step by using satellite data to make this reference dataset for China’s continental land area. Besides, most remotely-sensed fluxes and evapotranspiration product have null values in urban, water, snow, barren and desert areas, such as the studies of Mu et al., 2007, Wang et al., 2007 and Jiménez et al., 2009 (on page 14475, line 1-18). Here we have overcome the shortages of their dataset and produced a spatially continuous distributions of land-surface energy fluxes and evapotranspiration. The sentence was added to make this advancement more clearly for the readers to understand the importance of our work: ‘We have overcome the shortages of previous remotely-sensed evapotranspiration products which have null values in barren and desert areas.’. in the ‘conclusion and discussion’.

Finally, the critical challenge in using turbulent flux parameterization to remote sensing data is how to transfer from regional to continental and global scales (on page 14475, line 19-21). We have developed several steps to tackle the complexities met with the method when combining different spatial and temporal sampling input variables (on page 14480, line 13-30, page 14481, line 1-19). We also found a solution how to produce roughness length distribution for a continental area (On page 14475, line 25-29). Usually, the surface roughness length is given a fixed value in numerical models, here we developed a method to produce a dynamic variation of surface roughness length for the Chinese landmass which is closer to the reality. This novelty is notified by adding the paragraph in the ‘discussion and conclusions’:

‘We also found a solution on how to produce a dynamic surface roughness length due to variations in the canopy height, which is closer to the reality, for a continental area. Usually, the surface roughness length is given a fixed value in numerical models.’

2. Discussion of this paper is not organized well. Some of sentences are just the rewords of Introduction. Based on the validation results, I would like to see more general characteristics of the data sets. When and where the produced data is likely to fail or to deteriorate the accuracy? And why? What’s the bottleneck? Data or flux modellings? How could it be improved in future study?

Response: Thank you for pointing out these important issues for modellings. We agree that the assumptions and model imperfection are issues of importance. From the validation results, it shows that the sensible heat fluxes over high canopy is underestimated, this is due to the roughness sublayer over the high canopy is not considered in the model. So we added this sentence in the discussion part 'Additionally, the sensible heat flux over forest is underestimated by present turbulent flux parameterization method in SEBS which does not take the roughness sublayer over high canopy (Bosveld, 1999) into consideration.'

The bottleneck should be the availability of accurate remote sensing data, we have discussed partly on page 14492, line 14-19. To clarify the problem, we would like to add the sentences in the new manuscript to discuss it more and how the dataset may fail, 'The accuracy of turbulent heat fluxes is largely dependent on the remotely sensed land surface temperature. Here we have made an assumption that the averaged Aqua and Terra sensors sensed LST in each month can represent the monthly average LST. Terra satellite sensor passes twice a day (at about 10:30am, and 22:30pm local time), also the Aqua satellite passes twice a day (at about 01:30am, and 13:30pm local time). So MODIS have four samples each day. The samples may not be enough for calculating the monthly LST, also due to the cloud noise. Besides, the time period of MODIS datasets is not longer than 15 years which may limit application of our dataset in climate analysis.' following 'It is challenging tofrom half-hourly through to monthly.'

3. The authors use the term "turbulent heat flux". However, radiations like SWD, LWD are not considered turbulent heat flux. Rephrase it.

Response: Here we use 'turbulent heat flux' to represent sensible and latent heat. 'turbulent heat flux' was used two times in our paper. The first one is 'In our study we set out to estimate turbulent heat fluxes simulated with energy balance' and aerodynamic parameterization formulas that are based on a revised model of the surface energy balance system (SEBS)'. As this work is to calculate sensible and latent heat fluxes with SWD, LWD etc. which is produced by other works. So we think this is correct. The second usage is in the sentence 'Potential effects of changes in turbulent heat fluxes on the monsoon over East Asia (Lee et al., 2011)'. Lee et al. have analyzed the changes of sensible and latent heat impacts on the East Asia, so the sentence is also right.

4. Page 14472, line 16: "turbulent flux and evapotranspiration" sounds like a little weird. Latent heat flux is also one of the turbulent flux, so I would recommend using latent heat flux instead of evapotranspiration.

Response: We understand that the reviewer to pick 'turbulent flux and evapotranspiration' out from the background. Turbulent flux includes 'sensible and latent heat fluxes'. So we do not suggest to use 'turbulent flux and latent heat flux'. Here we use 'turbulent flux' and 'evapotranspiration' to relate two community, 'turbulent flux' refers to the land-air study, and evapotranspiration refers to water cycle and hydrological study. The accurate downward long-wave radiation datasets are needed for both area when using the surface energy balance method. So we prefer not to change this sentence.

5. Page 14486, Lines 3 – 7: I'm not sure that this comparison is meaningful and fair.

The regions of interests are different and some of data are global estimation.

Response: *Vinukollu et al. (2011b) could be the first and only one SEBS application in global fluxes and evapotranspiration efforts. We also contacted the authors to share their dataset with us, unluckily, due to disk physical problems, they can't share the dataset with us which make it impossible to do more detailed comparative analysis. Our paper also addresses how to produce a continental turbulent flux and evapotranspiration dataset with the model, but with an improved one. Due to there are so many common basis, we think the comparisons are useful. We agree that the forcing dataset are different. But, we and Vinukollu et al. have the same purpose—how to get more accurate global or continental heat fluxes and evapotranspiration. The lower RMSE could be due to the model improvement and more accurate forcing dataset used in our study. So we have added the sentence 'The difference could be due to the model improvement and more accurate meteorological forcing dataset used in our study.' to discuss the difference in RMSE values. This literature comparison is important for our conclusion that 'more accurate ... datasets are needed to be able to accurately estimate turbulent fluxes and evapotranspiration when using the surface energy balance model.'*

6. Table 3: please add the explanation of “MB” in the caption. “Mean bias”

Response: *We have added 'MB is mean of observation minus model simulation.' in the caption of new attached manuscript.*

Reference:

- Bosveld, F. C.: Exchange processes between a coniferous forest and the atmosphere, Ph.D, Wageningen University, 181 pp., 1999.
- Chen, F., Mitchell, K., Schaake, J., Xue, Y., Pan, H.-L., Koren, V., Duan, Q. Y., Ek, M., and Betts, A.: Modeling of land surface evaporation by four schemes and comparison with FIFE observations, *Journal of Geophysical Research: Atmospheres*, 101, 7251-7268, 10.1029/95jd02165, 1996.
- Chen, Y., Yang, K., He, J., Qin, J., Shi, J., Du, J., and He, Q.: Improving land surface temperature modeling for dry land of China, *J. Geophys. Res.*, 116, D20104, 10.1029/2011jd015921, 2011.
- Hogue, T. S., Bastidas, L., Gupta, H., Sorooshian, S., Mitchell, K., and Emmerich, W.: Evaluation and Transferability of the Noah Land Surface Model in Semiarid Environments, *Journal of Hydrometeorology*, 6, 68-84, 10.1175/jhm-402.1, 2005.
- Wang, A., Barlage, M., Zeng, X., and Draper, C. S.: Comparison of land skin temperature from a land model, remote sensing, and in-situ measurement, *Journal of Geophysical Research: Atmospheres*, 2013JD021026, 10.1002/2013jd021026, 2014.

Reviewer #2

Generally, this MS utilized multi-source data and a modified surface energy balance model to simulate the temporal and spatial patterns of surface energy fluxes at national scale (China). Compare to the previous related studies, a higher resolution data set of energy fluxes was produced and well validated with ground flux measurement. With such dataset, 10 years variations of radiation and turbulent heat fluxes in China were evaluated. Obviously, this study provided a useful dataset and gave some interesting results on the spatial-temporal patterns of land surface energy balance in China, especially in Tibetan Plateau. However, there are still some explanations and modifications are needed, 1. In Introduction section, if the authors can make a more clearly introduction on the reasons for constructing such a high spatial resolution and long term dataset at national scale? And what are the progresses about this topic in China and world?

RESPONSE: *Thanks for your precious comments and suggestions. As Reviewer #1 has pointed out that ‘the global surface energy flux data sets, including reanalysis data, do not have enough spatial and temporal resolution when looking at the national-level fluxes. The surface flux data sets from reanalysis data sets still contain large uncertainty. Therefore,it is necessary to produce spatially and temporal higher resolution surface flux data sets.’; We have also discussed this issue (why a high spatial resolution and long term dataset at national scale is necessary):*

On Page 14473, Line11-19 of our ACPD manuscript:

‘While it is of critical importance to understand the partitioning of water and energy distribution across China’s terrestrial surface, accurate monitoring of their spatial and temporal variation is notoriously difficult (Ma et al., 2011). Several field experiments are being carried out to monitor turbulent fluxes over selected land cover in China by using ground-based eddy covariance devices (Wang et al., 2010; Yu et al., 2006; Ma et al., 2008b; Li et al., 2009). However, these measurements are only representative of small areas around the locations where the measurements are being made. For this reason, establishment of an eddy-covariance flux network cannot provide a complete land-surface heat flux picture for the entire Chinese landmass.’ and

On Page 14474, line 8-14 of our ACPD manuscript:

‘Zhu et al. (2012) have also reported that summer sensible heat flux derived from eight datasets (including NCEP, ERA, and GLDAS) of China’s Tibetan Plateau region differ from each other in their spatial distribution. In addition, all the flux datasets mentioned above are based on model simulations, which have deficiencies for studying changes in water-cycle and land–air interactions in China (Chen et al., 2013; Su et al., 2013; Wang and Zeng, 2012; Ma et al., 2008a)’.

in the Introduction section.

We have reviewed the topic progress in world with these sentences on page 14473, line 20- page 14474 line 6 (ACPD manuscript): ‘A number of methods can be used to derive land-surface energy fluxes. Jung et al. (2009), for example, generated global spatial flux fields by using a network up-scaling method.When these products

were applied at continental scales, the different approaches resulted in large differences (Vinukollu et al., 2011; Jiménez et al., 2011; Mueller et al., 2011). ’.

In the revised manuscript, we have added more discussions on these issues to let the reader understand our work clearly. All the changes have been shown by the track change in the manuscript word file, which is uploaded as the supplementary file of our response to the reviewer comments.

2. In model description, although the structure and equations were detail introduced with many references, it is still not clearly that how the model was developed based on those references in this MS.

RESPONSE: Actually, the most development of the SEBS model by us have been done within our previous paper, Chen et al. JAMC 2013. The further development or improvement in this paper is to upscale the model to an continental coverage area. Actually, we have further developed several methods to help the model to be used in a global scale. Such as the method of how to get global canopy height information for SEBS. This method has been demonstrated in lines 16-30, page 14479 (ACPD manuscript). The second significant contribution of this work is how to make an gap filled land surface fluxes and evapotranspiration. Normally, application of remote sensing dataset is limited by the spatial and temporal gaps in themselves. Here we overcame the setbacks in LST product. To make this point more clearly, we added a new figure to show how reasonable is our process method of monthly LST.

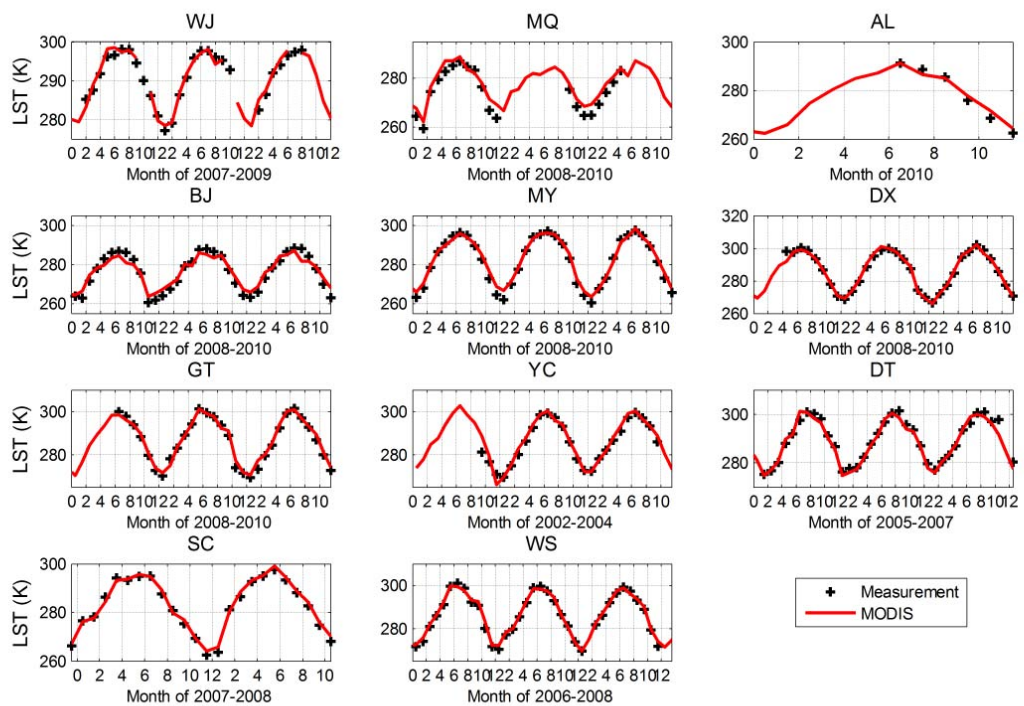


Fig. 3 Time series comparison of monthly averaged LST derived from MOD11C3&MYD11C3 and in-situ measurement.

Thus, Lines 22-30 on page 14482, line1-10 on page 14483 were also revised appropriately. Please check the new manuscript.

3. Only the EC data with more than 70% available in a month was acceptable in flux validation. However, it is popular that the most nighttime EC data usually was questionable and filtered out under weak turbulent condition, which resulted in large gaps in EC data. So 70% available data probably main come from daytime. If it will affect the monthly flux validation, for example, sensible heat flux?

RESPONSE: *We have checked the dataset, the percent of filtered fluxes at nighttime is very low, not higher than 0.1%. So its influence on the monthly averaged flux is negligible. 70% standard is used to kick off the months which have not enough samples due to equipment problems, e.g. EC at Maqu station has sensible heat flux data from 1th to 10th July, 2009, there is no data from 11th to 30th July due to electricity power problem, the valid sensible flux data takes a 30% percentage of that month. Thus the averaged monthly sensible heat flux for this month could not be used due to inadequate samples. That`s why we use this standard to filter this month and similar events at other stations.*

4. If possible, please add a figure to show the validation of LWD, because it was assumed to be important and there still existed room for improvement, although linear fitting slope and correlation coefficient attained 0.9 and 0.98, respectively.

RESPONSE: *If you look at the below evaluation results, it`s clear that the LWD has a certain systematic bias, even the R and fitting slope are very high. The scatter point closely located around the $0.91*x$ line, not 1:1 line, which makes us believe that the LWD still has some room for improvement. The following figure was added in the new manuscript. Please check the supplementary.*

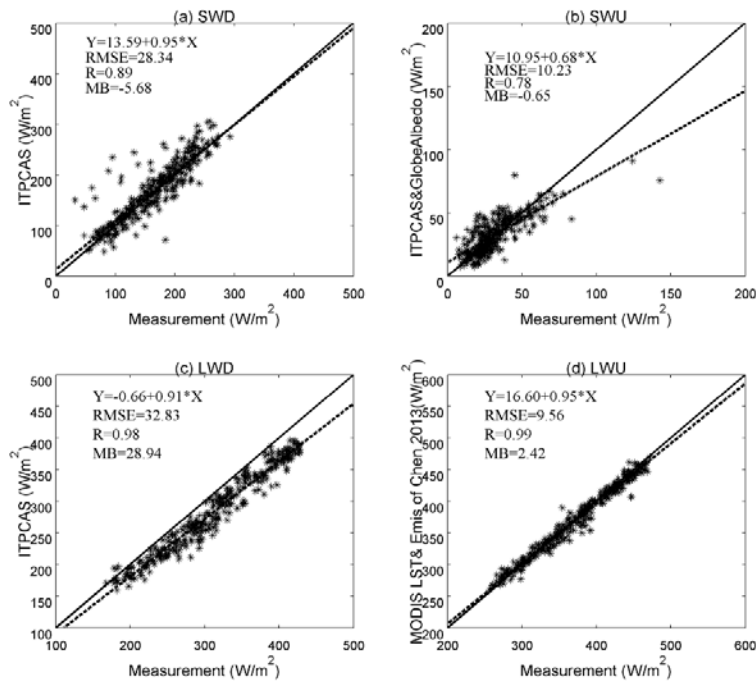


Figure 4 Scatter point for downward shortwave (SWD), upward shortwave (SWU) , downward longwave (LWD), and upward longwave (LWU) radiation against in-situ measurement.

5. Why only the validation from Yucheng and SC flux site were introduced in detail, the results were similar for other 9 sites?

RESPONSE: The validation results for other 9 sites were uploaded as supplementary of the ACPD paper. Here, we would like to list results for the three sites located in the Western, Eastern and center of Tibetan Plateau, to show part of the evaluation results. Please check for others in the supplementary materials of the discussion paper.

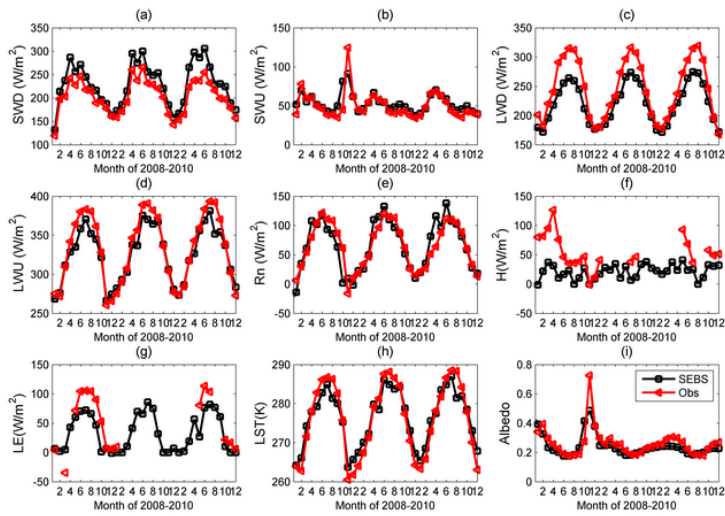


Fig. 1 SEBS input and output variables vs measurement at BJ station in the central Tibetan Plateau

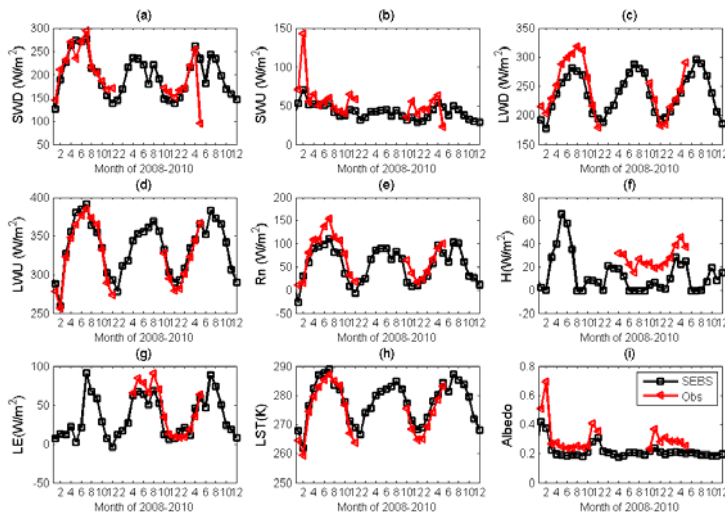


Fig. 2 SEBS input and output variables vs measurement at Maqu station in the eastern Tibetan Plateau

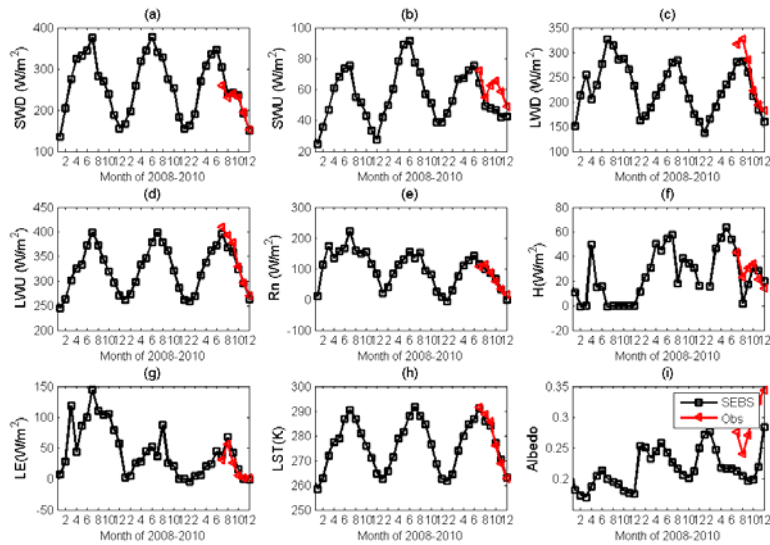


Fig.3 SEBS input and output variables vs measurement at Ali station in the western Tibetan Plateau

The validation results also show that the sensible heat fluxes over high canopy is lower estimated, this is due to that the roughness sublayer over the high canopy is not considered in the model. So we added this sentence in the discussion part, ‘Additionally, the sensible heat flux over forest is lower estimated by present turbulent flux parameterization method in SEBS which does not take the roughness sublayer over high canopy (Bosveld, 1999) into consideration.’.

6. In trend analysis, it is interesting for the distinct variations in Tibetan Plateau, for example, in Fig 9 and 10. Meanwhile, it is also noticeable that the radiation and turbulent energy fluxes decreased in both northeastern and north China. Related explanations will be helpful for the understanding of the spatial variations of radiation and fluxes in China as a whole picture.

RESPONSE: *Yes, we also agree that the trend analysis is interesting. The problem is that we only have 10-years dataset, which may not be long enough for climate studies. We have reminded the readers in the new manuscript with the sentence in the discussion section ‘. Besides, the time period of MODIS datasets is not longer than 15 years which has limited application of our dataset in climate analysis.’.*

Meanwhile, the dataset does show some variations in the last 10 years. We have reviewed papers and found some explanations, such as the drying atmosphere over the plateau could be used to explain why SWD on the Tibetan Plateau has increased during last decade, we also address the reason for the LWU rising trend in the Lhasa basin. It’s a pity that we didn’t find any related publications which could be used to explain the variations in radiation and fluxes in northeastern and north China.

7. The organization of discussion is not well, and lots of discussion has already appeared

in Introduction and Results section.

RESPONSE: *Thanks for your appreciated comments. We have revised the introduction and discussion section. We have added more detailed discussions about the reasons for constructing such a high spatial resolution and long term dataset for China land area. Please check the new manuscript.*

Technical corrections:

1. In Introduction section, some descriptions about the estimation method and input data were also included in this section, for example, “For this reason we chose a more physically-based method –turbulent flux parameterization – to produce the dataset” on p14475, line 17, and “To derive the surface energy balance terms for the Chinese landmass, we used high resolution reanalysis data, : :” on p14476, line 16. It will be more appropriate to move such description into the Methods section.

RESPONSE: *Please pay attention to the paragraph ‘The simple relationships established cannot give a reasonable approximation for extreme conditions such as bare soil or other types of non-canopy land cover (e.g. lakes, deserts) because land covers behave significantly differently in land-surface energy flux partitioning. Fortunately, turbulent flux transfer parameterization can overcome the shortcomings of statistical methods and produce spatially continuous distributions of land-surface energy fluxes with prepared meteorological forcing data. For this reason we chose a more physically-based method –turbulent flux parameterization – to produce the dataset..’, here we not only review the advancement in the related area, but also inform the readers why do we use the model. So we do not only talk about the Methods but also the frontier of land surface flux remote sensing retrievals. The two sentences you have selected out may not be enough to set up a new Methods section. The related paragraph was rewritten. We also revised the Introduction section. Please check the new manuscript.*

2. Canopy height is important for the estimation of land surface heat flux. From eq. 8, it was just the linear function of NDVI, and even canopy fraction (fc) from eq. 9. Although the author indicated the reference, if some HC validations at flux sites can be provided?

RESPONSE: *Actually, we have checked the produced canopy height at the 11 flux station by equation 8 and GLAS forest height. We add section 4.1 in the new manuscript to assess the canopy height method. The following content was added in the new version.*

“4.1 Canopy height assessment

We checked the canopy height variations at the 10 flux station produced by equation 8 and GLAS forest height (Figure 3). The derived canopy height for AL is not higher than 0.2 m, which is reasonable for the local land cover. YC, GT, and WS stations located in the North China, represent a typical agricultural land, where crops mature twice per year. The highest canopy height is around 1.5 m, a similar magnitude to the height of maize in summer. The step decrease in canopy height in June at these three stations is due to that wheat/maize is harvested and new seeds are sown during this period. This step variation in the canopy height also causes similar step changes in sensible and latent heat flux (shown by Fig. 5). Although the land cover near WJ station is crop, it is more surround by forest in a 10 km diameter. The GLAS forest height reflects this ground truth. These

canopy height assessments at the observation sites enable us to consider that the developed method in this work is an appropriate one for solving scarcity of canopy height information at a continental area. ”

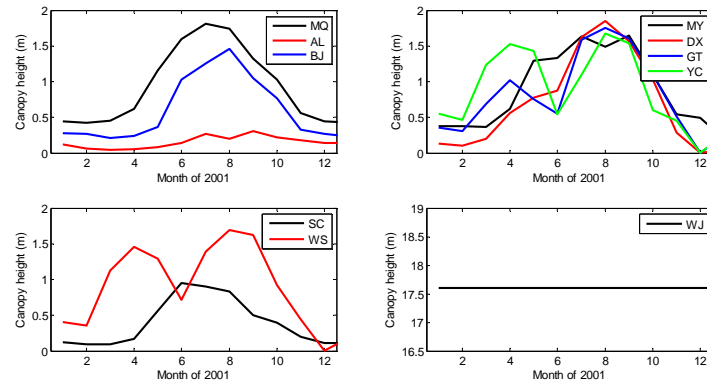
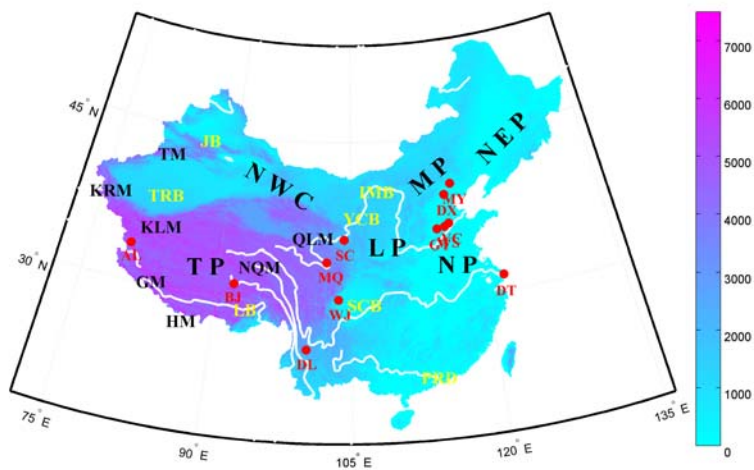


Fig. 3 Monthly variation of canopy height at the 10 flux stations

3. The color and letters in Fig.1 is confusing, please improve it.

RESPONSE: Figure 1 was changed to DEM map, please check the new figure:



4. From Table 3, it seems that no forest flux site was included for model validation.

RESPONSE: Yes, forest site was not included. However, we have evaluated the model with a forest flux site in Netherlands. It shows that the sensible heat flux over forest cover is lower-estimated by SEBS. We added the discussion to remind the readers about this

shortage 'Additionally, the sensible heat flux over forest is lower estimated by present turbulent flux parameterization method in SEBS which does not take the roughness sublayer over high canopy (Bosveld, 1999) into consideration.'

5. As for the sensible heat flux and latent heat flux, different names were used in this MS, for example, Heat flux, Surface fluxes, Heat and water fluxes, Land surface fluxes, Land surface-energy fluxes, Turbulent flux, Turbulent heat fluxes, Turbulent heat, etc., please check and uniform it.

RESPONSE: *A uniform 'land surface heat fluxes' was adopted in the new manuscript. Please check it.*

References:

- Bosveld, F. C.: Exchange processes between a coniferous forest and the atmosphere, Ph.D, Wageningen University, 181 pp., 1999.
- Chen, Y., Yang, K., Qin, J., Zhao, L., Tang, W., and Han, M.: Evaluation of AMSR-E retrievals and GLDAS simulations against observations of a soil moisture network on the central Tibetan Plateau, *Journal of Geophysical Research: Atmospheres*, 118, 4466-4475, 10.1002/jgrd.50301, 2013.
- Jiménez, C., Prigent, C., Mueller, B., Seneviratne, S. I., McCabe, M. F., Wood, E. F., Rossow, W. B., Balsamo, G., Betts, A. K., Dirmeyer, P. A., Fisher, J. B., Jung, M., Kanamitsu, M., Reichle, R. H., Reichstein, M., Rodell, M., Sheffield, J., Tu, K., and Wang, K.: Global intercomparison of 12 land surface heat flux estimates, *J. Geophys. Res.*, 116, D02102, 10.1029/2010jd014545, 2011.
- Jung, M., Reichstein, M., and Bondeau, A.: Towards global empirical upscaling of FLUXNET eddy covariance observations: validation of a model tree ensemble approach using a biosphere model, *Biogeosciences*, 6, 2001-2013, 10.5194/bg-6-2001-2009, 2009.
- Li, X., Li, X., Li, Z., Ma, M., Wang, J., Xiao, Q., Liu, Q., Che, T., Chen, E., Yan, G., Hu, Z., Zhang, L., Chu, R., Su, P., Liu, Q., Liu, S., Wang, J., Niu, Z., Chen, Y., Jin, R., Wang, W., Ran, Y., Xin, X., and Ren, H.: Watershed Allied Telemetry Experimental Research, *Journal of Geophysical Research: Atmospheres*, 114, D22103, 10.1029/2008jd011590, 2009.
- Ma, L., Zhang, T., Li, Q., Frauenfeld, O. W., and Qin, D.: Evaluation of ERA-40, NCEP-1, and NCEP-2 reanalysis air temperatures with ground-based measurements in China, *J. Geophys. Res.*, 113, D15115, 10.1029/2007jd009549, 2008a.
- Ma, Y., Zhong, L., Wang, B., Ma, W., Chen, X., and Li, M.: Determination of land surface heat fluxes over heterogeneous landscape of the Tibetan Plateau by using the MODIS and in situ data, *Atmos. Chem. Phys.*, 11, 10461-10469, 10.5194/acp-11-10461-2011, 2011.
- Ma, Y., Kang, S., Zhu, L., Xu, B., Tian, L., and Yao, T.: Tibetan Observation and Research Platform- Atmosphere-land interaction over a heterogeneous landscape, *Bull. Amer. Meteor. Soc.*, 89, 1487-1492, 10.1175/2008BAMS2545.1, 2008b.

Mueller, B., Seneviratne, S. I., Jimenez, C., Corti, T., Hirschi, M., Balsamo, G., Ciais, P., Dirmeyer, P., Fisher, J. B., Guo, Z., Jung, M., Maignan, F., McCabe, M. F., Reichle, R., Reichstein, M., Rodell, M., Sheffield, J., Teuling, A. J., Wang, K., Wood, E. F., and Zhang, Y.: Evaluation of global observations-based evapotranspiration datasets and IPCC AR4 simulations, *Geophys. Res. Lett.*, 38, L06402, 10.1029/2010gl046230, 2011.

Su, Z., de Rosnay, P., Wen, J., Wang, L., and Zeng, Y.: Evaluation of ECMWF's soil moisture analyses using observations on the Tibetan Plateau, *Journal of Geophysical Research: Atmospheres*, 118, 5304-5318, 10.1002/jgrd.50468, 2013.

Vinukollu, R. K., Meynadier, R., Sheffield, J., and Wood, E. F.: Multi-model, multi-sensor estimates of global evapotranspiration: climatology, uncertainties and trends, *Hydrol Process*, 25, 3993-4010, 10.1002/hyp.8393, 2011.

Wang, A., and Zeng, X.: Evaluation of multireanalysis products with in situ observations over the Tibetan Plateau, *J. Geophys. Res.*, 117, D05102, 10.1029/2011jd016553, 2012.

Wang, G., Huang, J., Guo, W., Zuo, J., Wang, J., Bi, J., Huang, Z., and Shi, J.: Observation analysis of land-atmosphere interactions over the Loess Plateau of northwest China, *J. Geophys. Res.*, 115, D00K17, 10.1029/2009jd013372, 2010.

Yu, G.-R., Wen, X.-F., Sun, X.-M., Tanner, B. D., Lee, X., and Chen, J.-Y.: Overview of ChinaFLUX and evaluation of its eddy covariance measurement, *Agricultural and Forest Meteorology*, 137, 125-137, <http://dx.doi.org/10.1016/j.agrformet.2006.02.011>, 2006.

Zhu, X., Liu, Y., and Wu, G.: An assessment of summer sensible heat flux on the Tibetan Plateau from eight data sets, *Science China Earth Sciences*, 55, 779-786, 10.1007/s11430-012-4379-2, 2012.

24 conditions (average bias = 15.3 Wm^{-2} , RMSE = 26.4 Wm^{-2}). The quality of the data product was
25 also assessed against the GLDAS dataset. The results show that our method is efficient for
26 producing a high-resolution dataset of surface energy flux for the Chinese landmass from
27 satellite data. The validation results demonstrate that more accurate downward long-wave
28 radiation datasets are needed to be able to accurately estimate turbulent fluxes and
29 evapotranspiration when using the surface energy balance model. Trend analysis of land-surface
30 radiation and energy exchange fluxes revealed that the Tibetan Plateau has undergone relatively
31 stronger climatic change than other parts of China during the last 10 years. The capability of the
32 dataset to provide spatial and temporal information on water-cycle and land-atmosphere
33 interactions for the Chinese landmass is examined. The product is free to download for studies of
34 the water cycle and environmental change in China.

35

36 **1. Introduction**

37 As China is one of the fastest growing and urbanizing economies in the world, changes in land
38 cover and land use can significantly influence the environment by altering land-atmosphere
39 energy and water exchanges (Suh and Lee, 2004;Lin et al., 2009). For instance, rapid urban
40 expansion has substantially changed [land](#) surface heat fluxes in the Pearl River delta (PRD) (Lin
41 et al., 2009) and has increased sensible heat fluxes in the Beijing metropolitan area (Zhang et al.,
42 2009a). The variability of surface energy balance and its partitioning may also have an important
43 impact on climate variability in China (Sun and Wu, 2001). Similarly, changes in surface energy
44 fluxes have been shown to alter the intensity of the East Asian monsoon (Zhou and Huang,
45 2008;Qiu, 2013;Hsu and Liu, 2003). In short, understanding variation in energy fluxes is

46 important for the study of climate change in China (Brauman et al., 2007). Nevertheless, the
47 spatial and temporal variability of China's land-surface energy balance, and the magnitude of
48 each, are still unknown.

49 While it is of critical importance to understand the partitioning of water and energy distribution
50 across China's terrestrial surface, accurate monitoring of their spatial and temporal variation is
51 notoriously difficult (Ma et al., 2011). Several field experiments are being carried out to monitor
52 turbulent fluxes over selected land cover in China by using ground-based eddy covariance
53 devices (Wang et al., 2010; Yu et al., 2006; Ma et al., 2008b; Li et al., 2009). However, these
54 measurements are only representative of small areas around the locations where the
55 measurements are being made. For this reason, establishment of an eddy-covariance flux
56 network cannot provide a complete land-surface heat flux picture for the entire Chinese landmass.

57 | A number of ~~methods can be used to products can be derived from~~ land-surface energy fluxes.
58 Jung et al. (2009), for example, generated global spatial flux fields by using a network up-scaling
59 method. However their flux network included only a limited number of flux stations in China.
60 The Global Soil Wetness Project 2 (GSWP-2) (Dirmeyer et al., 2006) produced a global land
61 surface product on a 1×1 degree grid for the period 1986 to 1995. The Global Land Data
62 Assimilation System (GLDAS) (Rodell et al., 2004) can provide a global coverage in the form of
63 3-hourly, 0.25-degree data. Furthermore, products from the European Centre for Medium-Range
64 Weather Forecasts (ECMWF) interim reanalysis (ERA-Interim) (Dee et al., 2011), the National
65 Centers for Environmental Prediction (NCEP) (Kalnay et al., 1996), Modern-Era Retrospective
66 Analysis for Research and Applications (MERRA) (Rienecker et al., 2011) and other reanalysis
67 data can also provide temporally continuous – but coarse – spatial resolution datasets of land

68 surface fluxes. Jiménez et al. (2011) made an inter-comparison of different land-surface heat flux
69 products. When these products were applied at continental scales, the different approaches
70 resulted in large differences (Vinukollu et al., 2011a; Jiménez et al., 2011; Mueller et al., 2011).

71 The problems met by using currently available flux data in climate studies of China have been
72 reported by Zhou and Huang (2010). Zhu et al. (2012) have also reported that summer sensible
73 heat flux derived from eight datasets (including NCEP, ERA, and GLDAS) of China's Tibetan
74 Plateau region differ from each other in their spatial distribution. In addition, all the flux datasets
75 mentioned above are based on model simulations, which have deficiencies for studying changes
76 in water-cycle and land-air interactions in China (Chen et al., 2013c; Su et al., 2013; Wang and
77 Zeng, 2012; Ma et al., 2008a).

78 A spatially and temporally explicit estimate of surface energy fluxes is of considerable interest
79 for hydrological assessments and meteorological and climatological investigations (Norman et
80 al., 2003). Satellite-sensed data of surface variables can be used to produce maps of heat and
81 water fluxes at different scales (Wang and Liang, 2008; Li et al., 2012a; Liu et al., 2010; Vinukollu
82 et al., 2011b). Remote sensing approaches to estimate surface heat and water fluxes have been
83 largely used on regional scales (Fan et al., 2007; Ma et al., 2011; Jia et al., 2012; Zhang et al.,
84 2009b; Li et al., 2012b; Shu et al., 2011), but there is no analysis of satellite-derived data currently
85 underway to produce a complete, physically-consistent, decadal land-surface heat flux dataset
86 (Jiménez et al., 2009) for the Chinese landmass. The use of remotely-sensed data offers the
87 potential of acquiring observations of variables such as albedo, land surface temperature, and
88 NDVI at a continental scale for China. ~~Figure 1 shows an example of an NDVI map for China.~~

89

90 Since surface fluxes cannot be directly detected by satellite-borne sensors, an alternative for
91 estimating continental water and energy fluxes can be derived by applying the aerodynamic
92 theory of turbulent flux transfer (Ma et al., 2011) or by establishing statistical relationships
93 between related satellite observations and land surface fluxes (Jiménez et al., 2009; Wang et al.,
94 2007). Most remotely-sensed latent heat flux or evapotranspiration products have null values in
95 urban, water, snow, barren and desert areas (Mu et al., 2007; Wang et al., 2007; Jiménez et al.,
96 2009). This is due to the lack of a uniform representation of turbulent exchange processes over
97 different types of land cover in their method. Meanwhile, the aerodynamic turbulent transfer
98 method can describe the flux exchange through changes in surface roughness length over
99 different land covers. Statistical methods establish relationships between satellite-sensed
100 observations (e.g. *NDVI*, *LST*, albedo) and land surface fluxes through various fitting techniques
101 (Wang et al., 2007). The simple relationships established cannot give a reasonable approximation
102 for extreme conditions such as bare soil or other types of non-canopy land cover (e.g. lakes,
103 deserts) because land covers behave significantly differently in land-surface energy flux
104 partitioning. Fortunately, turbulent flux transfer parameterization can overcome the shortcomings
105 of statistical methods and produce spatially continuous distributions of land-surface energy
106 fluxes with prepared meteorological forcing data. For this reason we chose a more physically-
107 based method – turbulent flux parameterization – to produce the dataset.

108 The challenge in using turbulent flux parameterization lies in the transition from regional to
109 continental and global scales, because meteorological data of high resolution (i.e. 1–10 km) are
110 not easily obtained for a large region. Recently, Chinese scientists have produced high resolution
111 meteorological forcing data that can be used in our study. Another issue is the complexity met
112 with the method when combining different spatial and temporal sampling input variables. This is

113 discussed in detail in Subsection 3.1. The last difficulty that has surrounded application of
114 turbulent flux parameterization at continental scales is the acquisition of roughness length. To
115 address this difficulty, we have developed a remote-sensing-based mixing technique to estimate
116 canopy heights at a continental scale and use the resulting canopy height dataset to derive, for the
117 very first time, the dynamic variation of surface roughness length for the Chinese landmass.

118 Complex topography (shown by Fig. 1) and climatic conditions in China make it very difficult to
119 obtain a clear picture of the distribution of energy and water fluxes with a high spatial resolution
120 over a relatively long period for such a large area. In our study we ~~set out to~~ estimate
121 ~~turbulent~~land-surface heat fluxes ~~simulated~~ with energy balance and aerodynamic
122 parameterization formulas ~~in that are based on~~ a revised model of the surface energy balance
123 system (SEBS) (Chen et al., 2013b; Chen et al., 2013a; Su, 2002; Timmermans, 2011); Previous
124 tests show that the revised model delivers better performance and improvements in cases where
125 the type of land cover in China is bare soil, short canopy or snow (Chen et al., 2013b; Chen et al.,
126 2013a). Sensible heat flux in SEBS was derived from the difference between surface temperature
127 and air temperature by using Monin–Obukhov similarity theory and bulk atmospheric boundary
128 layer similarity (Brutsaert, 1999), which parameterizes ground surface momentum and heat-
129 transfer coefficient maps to take into account surface roughness, canopy height, vegetation cover,
130 and meteorological stability (Su et al., 2001; Su, 2002; Chen et al., 2013b). The latent heat flux
131 can then be estimated from an energy balance model, assuming surface net radiation and ground
132 flux are known (Ma et al., 2002; Allen et al., 2011; Vinukollu et al., 2011b). We used high
133 resolution reanalysis data, which merges model outputs, remote sensing observations, and in-situ
134 measurements. In addition, we also assessed the accuracy of the surface energy balance terms

135 (net radiation, sensible heat, latent heat, and ground heat fluxes) and their climatic trends in the
136 preceding decade (2001–2010).

137 After defining the equations of the SEBS model (Section 2), we describe (in Section 3) the input
138 data and ground-truth measurements used in the study. Further, we assess the capacity of the
139 remote-sensing-based product to reproduce the range and variability of measured fluxes by
140 comparing them with in-situ flux tower measurements, followed by trend analysis of the spatial
141 patterns of the fluxes (Section 4). Concluding remarks are found in Section 5.

142

143 **2 Model description and development**

144 The surface energy balance system model known as SEBS (Su, 2002) uses aerodynamic
145 resistance to create a spatially coherent estimate of land surface heat fluxes. Some model inputs
146 can be obtained from remote sensing data, while others can be obtained from meteorological
147 forcing data (e.g. GLDAS, ERA and NCEP reanalysis data). The model's equations and the
148 required forcing variables are described in the remainder of this section.

149 The surface energy balance equation can be expressed as:

$$150 \quad Rn = G_0 + H + LE, \quad (1)$$

151 where Rn is the net radiation flux; G_0 is the ground heat flux, which is parameterized by its
152 relationship with Rn (Su et al., 2001); H is the sensible heat flux; and LE is the latent heat flux.

153 LE is computed by using the evaporative fraction after deriving the other three variables in
154 Equation 1 and taking into consideration energy and water limits (Su, 2002). As these fluxes were

155 produced with a monthly average temporal resolution, energy storage in vegetation is not
156 considered.

157

158 Net radiation flux is:

$$159 \quad Rn = (1 - \alpha) \times SWD + LWD - LWU, \quad (2)$$

160 where α is broadband albedo; SWD is downward surface short-wave radiation; and LWD and LWU
161 are downward and upward surface long-wave radiation, respectively.

162 Here satellite observed albedo is used. LWU is derived from land surface temperature (LST) using
163 the Stefan–Boltzmann law. Land surface emissivity is derived as described in Chen et al. (2013a).
164 LWD and SWD values are obtained from meteorological forcing data.

165

166 Sensible heat flux (H) is computed according to the Monin–Obukhov similarity theory (MOST):

$$167 \quad H = k u_* \rho C_p (\theta_0 - \theta_a) \left[\ln \left(\frac{z-d}{z_{0h}} \right) - \Psi_h \left(\frac{z-d}{L} \right) + \Psi_h \left(\frac{z_{0h}}{L} \right) \right]^{-1}, \quad (3)$$

168 where k is the von Karman constant; u_* is friction velocity; ρ is air density; C_p is specific heat for
169 moist air; θ_0 is the potential temperature at the ground surface; θ_a is the potential air temperature
170 at height z ; d is the zero plane displacement height; Ψ_h is the stability correction function for
171 sensible heat transfer (Brutsaert, 1999); and L is the Obukhov length. In our study θ_a was obtained
172 from meteorological forcing data and θ_0 was derived from Moderate Resolution Imaging
173 Spectroradiometer (MODIS) LST data. For more detailed information about u_* and the calculation
174 of L , see Su (2002) and Chen et al. (2013b).

175

176 The roughness height for heat transfer (z_{0h}) in Equation 3 is calculated as follows:

177
$$z_{0h} = \frac{z_{om}}{\exp(kB^{-1})}. \quad (4)$$

178 Using the fractional canopy coverage, kB^{-1} at each pixel can be derived according to the
 179 following modification of the equation described by Su et al. (2001):

180
$$kB^{-1} = f_c^2 \times kB_c^{-1} + f_s^2 \times kB_s^{-1} + 2 \times f_c \times f_s \times kB_m^{-1}, \quad (5)$$

181 where f_c is fractional canopy coverage and f_s is the fraction of bare soil in one pixel; kB_c^{-1} is the
 182 kB^{-1} of the canopy; kB_s^{-1} is the kB^{-1} of bare soil; and kB_m^{-1} is kB^{-1} for mixed bare soil and
 183 canopy. As kB^{-1} is the most important parameter in a MOST-based calculation of sensible heat
 184 flux, kB^{-1} has been updated by Chen et al. (2013b). The momentum roughness length used to
 185 calculate kB_s^{-1} was given a value of 0.004 (Chen et al., 2013b), and the heat roughness length of
 186 bare soil was calculated according to Yang et al. (2002). The new kB^{-1} gives a better performance
 187 than the previous version of kB^{-1} (Chen et al., 2013b; Chen et al., 2013a). Detailed evaluations of
 188 the new parameterization of kB^{-1} can be found in Chen et al. (2013b).

189 The roughness height for momentum transfer z_{om} in Equation 4 is derived from canopy height
 190 (HC), leaf area index (LAI) and the canopy momentum transfer model (Massman, 1997):

191
$$z_{om} = HC \times (1 - d/HC) \times \exp(-k \times \beta), \quad (6)$$

192
$$\beta = C_1 - C_2 \times \exp(-C_3 \times C_d \times LAI), \quad (7)$$

193 where $C_1 = 0.32$, $C_2 = 0.26$, and $C_3 = 15.1$ are model constants related to the bulk surface drag
 194 coefficient (Massman 1997). The three constants have been tested for several canopies (Chen et al.,
 195 2013b; Cammalleri et al., 2010) and evaluated as one of the best solutions for canopy turbulent-
 196 flux parameterization (Cammalleri et al., 2010). C_d is the drag coefficient, which typically equals
 197 0.2 (Goudriaan, 1977); d is displacement height, which is derived from HC and the wind speed
 198 extinction coefficient (Su, 2002; Su et al., 2001).

199

200 As Chen et al. (2013b) have pointed out, HC is vital for turbulent heat simulations, which makes
201 accurate estimation of HC for the Chinese landmass important for this study. A remote-sensing-
202 based canopy height method (Chen et al., 2013b) was further developed to estimate canopy height
203 distribution for the whole China [in this study](#). Simard et al. (2011) produced a global forest
204 canopy-height map using data from the Geoscience Laser Altimeter System (GLAS) aboard
205 ICESat (Ice, Cloud, and land Elevation Satellite). However, short-canopy (e.g. maize, rice, wheat)
206 height information cannot be acquired by laser techniques. Since short-canopy height usually
207 varies by season throughout the year – crops are planted in spring and harvested in autumn – we
208 calculated short-canopy height using an NDVI-based equation from Chen et al. (2013b):

$$209 \quad HC = HC_{min} + \frac{HC_{max} - HC_{min}}{(NDVI_{max}(x,y) - NDVI_{min}(x,y))} \times (NDVI(x,y) - NDVI_{min}(x,y)) ,$$

210 (8)

211 where HC_{max} and HC_{min} are the maximum and minimum short-canopy height; HC_{min} is set to
212 0.0012 m (Chen et al., 2013b); and HC_{max} is set to 2.5 m, corresponding to the greatest height of
213 seasonal crops in China. $NDVI_{min}$ and $NDVI_{max}$ are [a matrix of](#) minimum and maximum NDVI
214 values during our 10-year study period. Each short-canopy pixel was given an $NDVI_{min}$ and
215 $NDVI_{max}$ value to calculate the canopy height. The NDVI-based short-canopy height method
216 above was used to fill relevant pixels with forest canopy heights of less than 10 m. Higher
217 canopy heights (greater than 10 m) were assumed to be constant, i.e. with no seasonal change.
218 By merging canopy heights greater than 10 m and variable short-canopy data, we constructed
219 dynamic monthly maps of canopy heights for the Chinese landmass for the period of 2001–2010.

Formatted: Automatically adjust right indent when grid is defined, Space After: 10 pt, Adjust space between Latin and Asian text, Adjust space between Asian text and numbers

220 | These maps were then used to calculate [land surface](#) heat fluxes. [Figure 2 gives an example of](#)
221 [derived canopy height at 11 China flux stations.](#)

222

223 **3 Data and validation**

224 Our modeling approach makes use of a variety of satellite-based sensor data and meteorological
225 forcing data to estimate monthly energy and water fluxes across China. The forcing data can
226 come from satellite-based or reanalysis datasets. Due to the influence of weather, satellite-sensed
227 visible and thermal band data (e.g. NDVI, albedo, LST) often have spatial and temporal gaps in
228 daily data. Various temporal and spatial gap-filling algorithms have been developed to produce
229 continuous monthly data for satellite-sensed variables (Chen et al., 2004;Moody et al., 2005). In
230 order to avoid both spatial and temporal gaps in the final product, we selected some specific
231 satellite-sensed datasets for this study (see Table 1). Detailed information about each input
232 variable is described in following subsections.

233

234 The longest period covered by the forcing dataset is approximately 31 years; the shortest is about
235 10 years. Spatial resolution of the dataset varies from 0.01 to 0.25 degrees and its sample
236 frequency from 3 hours to 1 month. The meteorological forcing data developed by the Institute
237 of Tibetan Plateau Research, Chinese Academy of Sciences (hereafter referred to as ITPCAS
238 forcing data) (He, 2010) was constructed to study meteorological variation in China. ITPCAS
239 forcing data covers the entire landmass of China and has the highest temporal resolution among
240 the input datasets used. Other variables such as LST and albedo, for example, have coarser
241 temporal resolutions (monthly) and global coverage. When combining data of different spatial
242 and temporal resolutions, both spatial and temporal scaling issues need to be addressed.

243

244 Estimates of land-surface energy flux can be subject to large errors, due to bias in the
245 meteorological forcing input data. The spatial distribution of meteorological variables is closely
246 related to topography (Li et al., 2013). When interpolating meteorological input variables to finer
247 scales, these effects have to be accounted for (Sheffield et al., 2006), which goes beyond the
248 scope of our study. Therefore we chose to resample the satellite product of high spatial resolution
249 to a lower spatial resolution that matches the resolution of the meteorological input data. Also,
250 the meteorological data were averaged to monthly values that have the same temporal resolution
251 as the remotely-sensed input variables. ITPCAS forcing data provides us data of the highest
252 spatial resolution among the meteorological forcing data currently available (e.g. ERA-interim,
253 NCEP, GLDAS, MERRA). Taking into account of all these items, our aim was to produce a
254 monthly product of 0.1×0.1 degree resolution land-surface heat fluxes that contains neither
255 spatial nor temporal gaps and can be used to study seasonal and inter-annual variability in the
256 hydrological and energy cycles of China.

257

258 | **3.1 Input datasets and their validations**

259 | **3.1.1 Meteorological forcing data**

260 In studies previous to ours, reanalysis data have been applied in many different ways, for example
261 to construct land-surface forcing data (Sheffield et al., 2006), to detect climate trends (Taniguchi
262 and Koike, 2008), and to investigate water and energy cycles at regional and continental scales
263 (Roads and Betts, 2000). Reanalysis data has also been applied by the remote sensing community
264 to derive estimates of global terrestrial evapotranspiration and gross primary production (Mu et al.,
265 2007; Yuan et al., 2010). Few studies, however, have used reanalysis data together with remotely-

266 sensed ground data to derive global land-energy fluxes (sensible heat flux, latent heat flux, net
267 radiation, etc.).

268

269 Researchers have developed several kinds of reanalysis data. Comparisons and evaluations of
270 these reanalysis products with in-situ observations have been performed for individual sites,
271 specific regions, and the entire globe (Wang and Zeng, 2012; Decker et al., 2011). It is well known
272 that inaccuracies existing in reanalysis forcing data may have substantial impacts on the
273 simulation of land-surface energy partitioning. It is difficult to choose which reanalysis data is
274 better for use as forcing data. Additionally, the spatial resolution of all of the above
275 reanalysis/forcing datasets is not as high as that of remote sensing data. The ITPCAS forcing
276 dataset was produced by merging a variety of data sources. This dataset benefits in particular from
277 the merging of information from 740 weather stations operated by the China Meteorological
278 Administration that have not been used in other forcing data. The dataset has already been used to
279 run land surface models and has been shown to be more accurate than other forcing datasets (Chen
280 et al., 2011; Liu and Xie, 2013). ITPCAS meteorological forcing data include variables such as
281 instantaneous near-surface air temperature (T_a), near-surface air pressure (P), near-surface air
282 specific humidity (Q), near-surface wind speed (W_s) at a temporal resolution of 3 hours, 3-hourly
283 mean downward surface short-wave (SWD) and downward surface long-wave (LWD) radiation.
284 The time period covered is from 1979 to 2010; the spatial resolution has a grid size of 0.1×0.1
285 degrees.

286

287 | **3.1.2 MODIS11C3 land surface temperature processing**

288 MODIS (Moderate-resolution Imaging spectroradiometer) sensors have been used to produce
289 several global and continental scale LST datasets. MOD11C3 V5 and MYD11C3 V5 products
290 (Wan, 2009) are validated over a range of representative conditions with an average bias of less
291 than 1 Kelvin (Coll et al., 2009; Wan and Li, 2008). The MOD11C3 V5 monthly LST product,
292 MOD11C3 and MYD11C3, has a 0.05-degree grid size, a monthly temporal resolution without
293 gaps and covers the period March 2000 to October 2012 near present. It provides monthly daytime
294 and night-time LST values. In our study we averaged the daytime and night-time values of
295 MOD11C3 and MYD11C3 to represent monthly means.

296
297 After spatially interpolating the monthly MOD11C3 V5 mean LST from 0.05 × 0.05 degree to a 0.1
298 × 0.1 degree resolution, we picked out LST values of pixels that included the 11 flux tower
299 stations from which in-situ measurements were gathered. The time series comparisons of LST
300 with the ground measurements were shown by Fig. 2. It shows that the processed monthly LST
301 can present the seasonal variations in LST over different land covers very well. The pixel values
302 were validated against the in-situ LST measurements. Detailed information about each station is
303 given in Subsection 3.2. The linear correlation (R = 1.0), RMSE (= 1.9 K) and MB (mean value of
304 the satellite data minus in-situ observation = 0.5 K) indicate that the quality of the merged
305 remotely-sensed monthly LST data in China is high. They also show that MOD11C3 V5 LST
306 captures the in-situ LST variability of different elevations and land surfaces, which is described in
307 Subsection 4.1.

309 3.1.3 Albedo

310

Formatted: Font color: Auto

Formatted: Font: 12 pt

Field Code Changed

Field Code Changed

Formatted: Font color: Auto

Formatted: Font color: Auto

311 Land surface albedo determines the fraction of short-wave radiation absorbed by the ground, thus
312 influencing the surface energy budget. Studies of land-surface energy balance require temporal
313 and spatial albedo input data without gaps. Several research projects have been devoted to
314 producing long-term time series of surface albedo from various satellite-borne sensors (Riihel et
315 al., 2013;Muller et al., 2012;Liu et al., 2013a). However most of the albedo products do not
316 provide gap-filled time-series albedo maps. Taking MODIS MCD43B albedo product as an
317 example, 20 to 40% of the pixels of global landmass miss valid albedo values every year (Liu et
318 al., 2013a). Twenty percent invalid values in albedo input data will result in the same amount of
319 empty values in ~~heat flux~~ output, an issue that limits albedo data that can be used in our study.
320 After checking several albedo products (including GlobAlbedo (Muller et al., 2012), CMSAF
321 cClouds, Albedo and RAdiation Surface Albedo (CLARA-SAL albedo) (Riihel et al., 2013), and
322 MCD43B), we decided to use GlobAlbedo as its data does not contain spatial or temporal gaps.
323 This albedo dataset is based on a monthly sample and has a spatial resolution of 0.05 degrees,
324 which we interpolated to a 0.1 degree resolution for our study.

325

326 **3.1.4 NDVI**

327 The Normalized Difference Vegetation Index (NDVI) is regarded as a reliable indicator of
328 vegetation parameters. NDVI has been widely used to explore vegetation dynamics and their
329 relationships with environmental factors (Piao et al., 2006). NDVI data from the Systeme Pour
330 l’Observation de la Terre (SPOT) VEGETATION sensor, distributed by Vito, have a spatial
331 resolution of 1 km × 1 km and a temporal resolution of 10 days (synthesized on days 1, 11 and
332 21 of each month). In order to reduce noise resulting from clouds, the maximum NDVI value in
333 a month for each pixel is selected to represent the canopy status of that month.

334

335 | 3.1.5 Canopy fraction

Formatted: Font color: Red

336 Canopy fraction (f_c) is defined as the fraction of ground surface covered by the vegetation
337 canopy (varying from 0 to 1). f_c in SEBS is used to distinguish the contributions of vegetation
338 and soil to the roughness parameterization. Here f_c was derived from NDVI data using the
339 following equation:

$$f_c = \frac{NDVI - NDVI_{min}}{NDVI_{max} - NDVI_{min}} .$$

340 3.2 Validation data

341 The product generated by our model needed to be validated by comparing it with an independent
342 observational dataset. The energy balance measurement system (eddy covariance, four
343 component radiation and ground heat flux) at flux sites is widely accepted as a method for direct
344 measurement of energy and fluxes and is widely applied for assessing global evapotranspiration
345 products (Zhang et al., 2010;Jung et al., 2011;Yan et al., 2012;Fisher et al., 2008).

346 To validate the product, we compiled a dataset from 11 flux stations in China with land cover
347 types including bare soil, alpine meadow, forest, cropland, orchard, grassland, and wetlands.
348 Elevations of these stations range from 5 m to 4800 m. The observational dataset includes data
349 from Maqu (MQ) (Chen et al., 2013b;Wang et al., 2013), Wenjiang (WJ) (Zhang et al., 2012),
350 Bijie (BJ) (Ma et al., 2006), Miyun (MY) (Liu et al., 2013b), Daxing (DX) (Liu et al., 2013b),
351 Guantao (GT) (Liu et al., 2011;Liu et al., 2013b), Yucheng (YC) (Flerchinger et al., 2009),
352 Dongtan (DT) (Zhao et al., 2009), SC (Semi-Arid Climate and Environment Observatory of
353 Lanzhou University) (Huang et al., 2008;Wang et al., 2010;Guan et al., 2009), and Weishan (WS)
354 stations (Lei and Yang, 2010b, a). Detailed information about each site is listed in Table 2.

355 Half-hourly fluxes were processed using standardized quality control procedures, which are
356 described in the literature references for each station. The half-hourly H, LE, and four
357 component radiation were then averaged to monthly values. Monthly average values derived
358 from less than 70% of the flux data in each month were not used in the validations. Gap filling
359 was not used for the flux measurement data.

360 4 Results

361 4.1 Canopy height assessment

362 We checked the canopy height variations at the 10 flux station produced by equation 8 and GLAS
363 forest height (Figure 3). The derived canopy height for AL is not higher than 0.2 m, which is
364 reasonable for the local land cover. YC, GT, and WS stations located in the North China,
365 represent a typical agricultural land, where crops mature twice per year. The highest canopy
366 height is around 1.5 m, a similar magnitude to the height of maize in summer. The step decrease
367 in canopy height in June at these three stations is due to that wheat/maize is harvested and new
368 seeds are sown during this period. This step variation in the canopy height also causes similar
369 step changes in sensible and latent heat flux (shown by Fig. 5). Although the land cover near WJ
370 station is crop, it is more surround by forest in a 10 km diameter. The GLAS forest height
371 reflects this ground truth. These canopy height assessments at the observation sites enable us to
372 consider that the developed method in this work is an appropriate one for solving scarcity of
373 canopy height information at a continental area.

374 4.2 Validation against flux tower measurements

Formatted: Font: Times New Roman, 12 pt, Bold

Formatted: List Paragraph, Outline numbered + Level: 2 + Numbering Style: 1, 2, 3, ... + Start at: 1 + Alignment: Left + Aligned at: 0 cm + Indent at: 0.85 cm

Formatted: Font: Times New Roman, 12 pt

Formatted ... [1]

Formatted ... [2]

Formatted ... [3]

Formatted ... [4]

Formatted ... [5]

Formatted ... [6]

Formatted ... [7]

375 The accuracy of remote-sensing-based land-surface heat fluxes is questionable without validation
376 against ground-based measurements (Meir and Woodward, 2010). This subsection describes the
377 validation of the SEBS model against heat flux measurements from a diverse range of climates.

378 In order to analyze the source of flux calculation errors, variables related to surface radiation
379 fluxes were all validated against flux station observations. Table 3 shows that H and LE have
380 RMSE values slightly less than 22 W/m^2 , which is lower than the RMSE values of products of
381 other statistical methods (see Table 7 in (Wang et al., 2007) and Table 5 in (Jiménez et al.,
382 2009)). Indeed, Kalma et al. (2008) assessed 30 published LE validation results obtained by
383 using ground flux measurements and reported an average RMSE value of about 50 W/m^2 and
384 relative errors of 15–30%. The RMSE of our LE dataset is significantly lower than their
385 averaged RMSE value.

386 We also compared our validation results with that of other, similar products produced by a
387 previous version of SEBS. Vinukollu et al. (2011b), for instance, produced global land surface
388 fluxes with RMSE values of 40.5 W/m^2 (sensible flux) and 26.1 W/m^2 (latent flux) (calculated
389 from Table 4 in (Vinukollu et al., 2011b)), which are larger than those in our study. The
390 difference could be due to the model improvement and more accurate meteorological forcing
391 dataset used in our study. Table 3 lists the values of the statistical parameters for the validation of
392 a data product produced by GLDAS (which has the highest spatial resolution compared with
393 other available terrestrial energy-flux datasets) against the same measurements from the Chinese
394 flux stations as used in our study. According to the mean values of the statistical variables, the
395 quality of our flux dataset is comparable to GLDAS' model and data assimilation results. These

396 comparisons of accuracy demonstrate that our revised model is efficient for producing a high-
397 resolution dataset of land-surface energy fluxes for China.

398 Net radiation has relatively higher RMSE and MB values than H , LE and G_0 in the dataset
399 because its accuracy is dependent on the accuracy of the other variable estimates (albedo, LST,
400 SWD, LWD, LWU, etc.). Any errors in these variables can cause bias in net radiation. LWD, for
401 example, has a linear-fitting slope value of 0.9, with most points located around the fitting line
402 (Figure 4). The correlation coefficient is as high as 0.98, thus demonstrating that there is still
403 room for improvement of the LWD algorithms. LWD in ITPCAS was calculated with algorithms
404 developed from measurements from across the Tibetan Plateau. The LWD algorithms may not,
405 therefore, be accurate for other parts of China (K. Yang, personal communication). This
406 underlines the need for more accurate LWD radiation fluxes in order to improve the accuracy of
407 turbulent fluxes and evapotranspiration.

408 In addition to the statistical evaluation of model results against observations, seasonal and inter-
409 annual changes in the model results also need to be checked. Yucheng station, which is an
410 agricultural experimental station with winter wheat and summer maize as dominant crops was
411 taken as an example (Figure 52). Crops at Yucheng station mature twice per year, which is
412 representative of warm temperate farming cropland, typical for the North China Plain. A two-
413 year flux dataset was used to compare against values extracted from our model-derived product.
414 The inter-annual and seasonal LST and LWU data closely match the in-situ observations. The
415 SWD term also successfully captures seasonal variations. LWD is systematically lower than
416 observations. The LE produced at Yucheng station not only captures seasonal variation, but also
417 responds at step stages, which occur when the wheat is harvested or maize seeds have just been

Formatted: Font: Not Italic

Formatted: Font: Not Italic

Formatted: Font: Not Italic

418 sown (from June to August). The increased sensible heat and decreased latent heat flux observed
419 in July 2003 were caused by the wheat harvest, however this signal change is not captured by the
420 model result. The simulated sensible and latent heat produced by SEBS has a one-month lag
421 when compared to reality. This phenomenon is caused by adopting a maximum monthly NDVI
422 value, resulting in faulty representation of canopy status changes in the month of June.

423 The Semi-Arid Climate and Environment Observatory of Lanzhou University (SC station) is
424 situated on China's Loess Plateau, at 1965.8 m above sea level. Annual mean precipitation there
425 is 381.1 mm and annual evapotranspiration is 1528.5 mm (Huang et al., 2008). Being typical of
426 stations operating under arid conditions, its flux measurements were compared with the grid
427 point values extracted from the model product (Figure 63). In 2008 the land surface around the
428 station was covered by snow from 19 January to 20 February. Consequently the GlobAlbedo
429 value was high for February. Unexpectedly, albedo was relatively low for January, which could
430 be caused by the coarse temporal sampling of the station pixel by the satellite sensor. The
431 calculated monthly sensible heat and latent heat in January 2008 have biases of -11.7 (with an
432 observed monthly mean sensible heat = 15 W/m²) and -7.6 W/m² (with an observed monthly
433 mean latent heat = 4.8 W/m²), respectively. The relatively large bias for SC station when
434 covered with snow may be caused by the mixed pixel around the station.

435 The results of other stations have been included in supplementary materials submitted with this
436 paper. Comparison with the results of these other stations shows that model estimates of surface
437 energy balance variables match the magnitude and seasonal variation observed at stations in
438 several contrasting ecosystems. Comparisons between the flux-tower-measured and the modeled
439 fluxes show that latent fluxes were more accurate than sensible fluxes. Comparisons with other

440 studies, which are presented in Table 4, show that the accuracy of our dataset is one of the best
441 among high-resolution datasets of land surface fluxes.

442

443 **4.3.2 Spatial distribution of land-surface energy fluxes.**

444 Using maps of average annual land-surface radiation and energy fluxes, we analyzed the spatial
445 patterns of radiation and energy fluxes for the Chinese landmass and compared them with other
446 products, such as GLDAS. The highest values of downward surface solar radiation (Figure 74a)
447 are located in the southwest of the Tibetan Plateau, while the lowest values occur in the Sichuan
448 Basin (SB). The highest levels of upward short-wave radiation (Figure 74c) occur around the
449 snow-covered peaks of the Himalaya (HM), Karakorum (KRM) and Kunlun (KLM), and the
450 Qilian (QLM) and Nyainqentanglha (NQM) mountain ranges. The strongest net solar radiation
451 (SWD minus SWU) on the Chinese landmass occurs in the southern part of the Tibetan Plateau
452 (see supplementary materials). The downward and upward long-wave radiation (Figures 74b and
453 74c) on the Tibetan Plateau are the lowest for the entire Chinese landmass. Southern China has
454 the highest levels of upward and downward long-wave radiation. The highest values of net long-
455 wave radiation (LWU minus LWD) occur in the southern and western parts of the Tibetan
456 Plateau (see supplementary materials).

457 Figure 85 shows that northwestern China (NWC), the western Tibetan Plateau (TP), the inner
458 Mongolian Plateau (MP) and the Loess Plateau (LP) have the highest yearly average values for
459 surface sensible-heat flux. Croplands of the northern China Plain (NCP, including the lowlands
460 of Shandong, Henan, and Hebei provinces) and the northeastern China Plain (NEP, including the

461 lowlands of Liaoning, Jilin, and Heilongjiang provinces) have low average yearly values for
462 sensible heat flux. The Pearl River delta (PRD) and Tarim (TRB) and Sichuan (SCB) basins also
463 have low levels of sensible heat flux, as do the Yinchuan (YCB) and the inner Mongolian basins
464 (IMB) along the Yellow River. This spatial distribution is consistent with GLDAS results (see
465 supplementary materials).

466 Simulated annual latent heat fluxes (Figure 85b) exhibit a southeast to northwest decreasing
467 gradient, which is consistent with other studies (Liu et al., 2013c). The southeastern Tibetan
468 Plateau has high levels of annual latent heat flux. The Gobi desert, in the northwest of China
469 (NWC), has the lowest annual latent heat flux, followed by the western Tibetan Plateau and the
470 inner Mongolian Plateau (MP). Lake regions along the Yangtze River and the region of basins
471 along the Yellow River have relatively high levels of latent heat flux.

472 The highest levels of annual average surface net radiation (Figure 85c) can be found in
473 southwestern China and the Lhasa Basin (LB); the lowest levels occur in the Sichuan (SCB)
474 and Junggar Basins (JB). The highest levels of annual average ground-heat flux (Figure 85c) are
475 to be found in western China, due to large amounts of incoming solar radiation that occur under
476 dry conditions. The monthly average of G0 is negligible when compared with other fluxes.

477 The role of plateau heating on Asia's monsoons is being discussed vigorously (Qiu, 2013; Wu et
478 al., 2012; Boos and Kuang, 2010). Figure 96 shows seasonal comparisons of H between boreal
479 winter (DJF), spring (MAM), summer (JJA) and autumn (SON). The largest area of positive
480 sensible heating occurs in spring. Lee et al. (2011) have shown that contrasting sensible heat
481 fluxes between the Chinese landmass and the seas surrounding it during the pre-monsoon period
482 (April-May) affect monsoon development in East Asia. Figure 96 (a) shows that sources of

483 sensible heating in spring occur over the Tibetan and several other plateaus in China. During
484 summer, the highest sensible heat fluxes are to be found on the western Tibetan Plateau, the
485 eastern Loess Plateau (LP) and in northwestern China (NWC).

486 LE in summer has the largest area of high latent heating, followed by that in spring, autumn and
487 winter (Figure 107). Latent heat in summer is highest in southeastern and southern China as a
488 result of abundant rainfall in these regions. Similarly on irrigated land, such as that found in
489 Yinchuan (YB), the inner Mongolian basin (IMB) and the downstream basins of the Tianshan
490 (TM) and Kunlun (KLM) mountains, latent heat and evapotranspiration are high due to the
491 ample supply of water in summer. Latent heat fluxes in autumn and winter are significantly
492 lower than those of the other two seasons. The magnitudes and spatial patterns of LE in China of
493 our product are generally consistent with other reports (Yao et al., 2013; Mu et al., 2007; Jung et
494 al., 2010).

495 Net radiation in summer has the highest values of the four seasons. Most of the Chinese
496 landmass acts as a source of surface energy for the atmosphere (Figure 118).

497

498 **4.43 Trend analysis**

499 The ability to capture the inter- and intra-annual variation for each land-surface energy variable
500 is of interest to researchers of monsoon phenomena and climate change (Zhu et al., 2012). Indeed,
501 understanding these variations is essential for studies on climate change and water-resource-
502 related issues. We have calculated annual average values for each flux variable. The
503 nonparametric Mann-Kendall test (MK) is one of the most widely used methods for hydro-

504 meteorological time series analysis (Liu et al., 2013d; Gan, 1998). The MK method was applied
505 to the series of annual average fluxes to check variations during the period 2001–2010. The
506 resulting slope indicates that downward surface short-wave radiation increased during that
507 decade over the majority of the Tibetan Plateau (Figure 129).

508 The ground solar measurements at China Meteorological Administration (CMA) stations during
509 2003–2006, as shown in Figure 1b of Yang et al. (2012), confirms the increasing trend of
510 downward surface short-wave radiation found in our study. The annual mean visibility measured
511 at these stations also displays an increasing trend (Figure 2a of Yang et al. (2012)), while ERA-
512 40 reanalyzed precipitable-water and station-observed specific humidity show a decreasing trend
513 from 2000 to 2006 (Figure 3a of Yang et al. (2012)). These results indicate that the atmosphere
514 over the plateau is becoming drier, which would explain why SWD has increased during the
515 decade.

516 The upward short-wave radiation over the Himalaya (HM), the Ganges (GM), the Karakorum
517 (KRM), and the Qilian (QLM) and Nyainqentanglha (NQM) mountain ranges has also increased
518 over the last 10 years, which may be caused by the glacial retreat that has occurred in these areas
519 (Scherler et al., 2011; Yao et al., 2004). Lhasa basin (LB) has the steepest rising trend in LWU,
520 perhaps because of the relatively greater degree of anthropogenic (e.g. urbanization) activity
521 occurring in this area. The trend analysis did not reveal any clear spatial pattern in downward
522 long-wave radiation. Net radiation over several high mountain ranges (including the Himalaya,
523 the Ganges, the Karakorum and the Qilian and Nyainqentanglha mountain ranges) increased by
524 approximately 5 W/m^2 between 2001 and 2010 (Figure 130). The strongest increase in net
525 radiation occurred in the central part of the Tibetan Plateau. As Matthew (2010) has pointed out,

526 soil moisture in the central Tibetan Plateau showed an increasing trend from 1987 to 2008.
527 Wetter soil can cause the ground surface to absorb more net radiation and thus increase latent
528 heat flux. Moreover, wetter soil can increase soil heating capacity (Guan et al., 2009) and so
529 further increase ground heat flux. The increases in net radiation and soil moisture may also
530 explain a rising trend in latent heat in the central Tibetan Plateau. Clearly, the plateau is
531 experiencing accelerated environmental changes (Zhong et al., 2011; Salama et al., 2012). Indeed,
532 land-surface radiation and energy trend analyses also show that the Tibetan Plateau is
533 experiencing a relatively stronger change in land-surface radiation (verified by Tang et al. (2011)
534 and energy exchange than other parts of China.

535

536 **5 Conclusions and discussion**

537 In view of China's highly fragmented landscape, high-resolution land-surface heat flux maps are
538 necessary for hydrological studies. As China includes arid, semi-arid, humid, and semi-humid
539 regions, quantifying its water and energy budgets is a challenge. We have developed the surface
540 energy balance system (SEBS) further to produce a land-surface heat flux dataset at a continental
541 scale of higher resolution than datasets derived using other methods. Generally, the global
542 surface energy flux data sets, including reanalysis data, do not have enough spatial and temporal
543 resolution when looking at the national-level fluxes. The surface flux data sets from reanalysis
544 data sets still contain large uncertainty, partly due to the deficiency in their land surface process
545 model that simulate land surface temperature by solving soil thermal transport equations (Chen
546 et al., 1996) and usually result in a large error in LST simulation (Chen et al., 2011; Wang et al.,
547 2014), if the model is not properly calibrated by measurements (Hogue et al., 2005). So the

Formatted: Font: (Default) Times New Roman, Not Italic

548 hypothesis tested in this paper is if it is possible to neglect the complex process in the soil by
549 using satellite observed land surface temperature directly to calculate the land surface fluxes at
550 continental scale? This study has demonstrated a benchmark on how to use satellite to derive a
551 land surface flux dataset for a continental area on a personal laptop which is absolutely not
552 feasible for the land surface process modeler to do in such a time and resource economic way.
553 We have overcome the shortages of previous remotely-sensed evapotranspiration products which
554 have null values in barren and desert areas. We also found a solution on how to produce a
555 dynamic surface roughness length due to variations in the canopy height, which is closer to the
556 reality, for a continental area. Usually, the surface roughness length is given a fixed value in
557 numerical models. In summary, using remote sensing data and surface meteorological
558 information, an independent data product of monthly resolution has been developed for land-
559 surface heat flux analysis. We have validated our remote-sensing-based approach with in-situ
560 observations from 11 flux stations in China. Taking into account the limitations of available
561 spatial data and computing resources, we applied the model to the entire Chinese landmass using
562 a 0.1-degree resolution meteorological dataset, MODIS LST, vegetation indices and other
563 variables to generate a climatological dataset of land-surface energy balance for a 10-year period.
564 The modeling results for both pixel-point and spatial distribution demonstrate that this approach
565 meets our aims in terms of (a) being robust across a variety of land cover and climate types and
566 (b) performing well for the temporal and spatial scales of interest. The spatial distribution maps
567 generated for each variable of surface energy balance give important background information on
568 the terrestrial hydrology and energy cycles. This product also demonstrates the impact of
569 topography and climatic conditions on land–air energy and moisture exchanges in China.

Formatted: Font: (Default) Times New Roman, Not Italic

Formatted: Font: (Default) Times New Roman, Not Italic

570 The applicability of remote-sensing-based estimates of land surface fluxes is hampered by
571 limited temporal coverage of satellite sensors (Ryu et al., 2012). Remote sensing data are
572 snapshots of the land surface status at a particular point in space and time (Ryu et al., 2011). It is
573 challenging to compare remote-sensing-based monthly flux data with ground measurements that
574 are made on time scales ranging from half-hourly through to monthly. The accuracy of land
575 surface heat fluxes is largely dependent on the remotely sensed land surface temperature. Here
576 we have made an assumption that the averaged Aqua and Terra sensors sensed LST in each
577 month can represent the monthly average LST. Terra satellite sensor passes twice a day (at about
578 10:30am, and 22:30pm local time), also the Aqua satellite passes twice a day (at about 01:30am,
579 and 13:30pm local time). So MODIS have four samples each day. The samples may not be
580 enough for calculating the monthly LST, also due to the cloud noise. Besides, the time period of
581 MODIS datasets is not longer than 15 years which may limit application of our dataset in climate
582 analysis. Additionally, the sensible heat flux over forest is underestimated by present turbulent
583 flux parameterization method in SEBS which does not take the roughness sublayer over high
584 canopy (Bosveld, 1999) into consideration.

Formatted: Font: Not Bold

Formatted: Font: Not Bold

585 The energy flux product we have developed has a spatial resolution of approximately 10 km,
586 while flux towers have a footprint of tens to hundreds of meters. The tower footprint may not be
587 representative of the larger pixel of the product, and this mismatch will result in errors if the
588 mean of the satellite pixel is different from that of the flux tower footprint. Remote-sensing-
589 based studies stress that direct comparison is a challenge because scale mismatch (Norman et al.,
590 2003) and heterogeneity of the land surface reduce the spatial representativeness of ground-site
591 measurements (Mi et al., 2006). Another challenge is validating the grid-box-based simulation

592 results on the scale of the Chinese landmass, since reliable observations of flux data are only
593 available from a few sites in the simulated region.

594 Potential effects of changes in ~~turbulent~~land surface heat fluxes on the monsoon over East Asia
595 (Lee et al., 2011) as a result of China's recent urbanization can be studied further using our
596 product. As an independent satellite-based product, it can also be used as a data source for
597 evaluating land surface models. We also produced an evapotranspiration product for China land
598 area using the dataset in this paper. The land surface fluxes and evapotranspiration product can
599 be downloaded from the URL. Recent result will be shared when the forcing dataset is available:
600 <https://drive.google.com/folderview?id=0B7yGrB1U9eDec2JFbnA5eldlVHc&usp=sharing>

601

602

603

604 **Acknowledgements**

605 This study was supported by the Chinese National Key Program for Developing Basic Sciences
606 (2010CB951701), the Chinese National Natural Science Foundation (41275010), CAS-KNAW
607 joint PhD project, the ESA WACMOS project and the FP7 CORE-CLIMAX project. The forcing
608 dataset used in our study was developed at the Data Assimilation and Modeling Center for
609 Tibetan Multi-spheres, Institute of Tibetan Plateau Research, Chinese Academy of Sciences. We
610 thank Professor Yang Kun for his comments during the writing of this paper. For our study we
611 used eddy covariance data acquired from the scientific community and networks. We

Formatted: Normal, Justified, Line
spacing: Double

612 acknowledge Wenjiang, Ali, Yucheng, and Weishan stations,
613 Nagqu Station of Plateau Climate and Environment, Magqu Zoige Plateau Wetlands Ecosystem
614 Research Station, and the Semi-Arid Climate and Environment Observatory of Lanzhou
615 University for providing their in-situ measurement datasets. We also acknowledge Professor
616 Xiangde Xu (CMA), Dr. Lide Tian (ITP, CAS), Dr. Yu Zhang (CAREERI, CAS), Dr. Shouhua
617 Xu (IGSNRR, CAS), Dr. Bin Zhao (Fudan University), and Dr. Huimin Lei (Tsinghua University)

618 for providing us with their flux datasets. Special thanks to the editor, Dr. Nobuko Saigusa, for her
619 kind help during the collection of Chinaflux network dataset.

Formatted: Font: Times New Roman, 12 pt

Formatted: Font: Times New Roman, 12 pt

Formatted: Font: Times New Roman, 12 pt

620

621

622

623

624

625

626

627

628

629

630

631 **References**

- 632 Allen, R., Irmak, A., Trezza, R., Hendrickx, J. M. H., Bastiaanssen, W., and Kjaersgaard, J.:
633 Satellite-based ET estimation in agriculture using SEBAL and METRIC, *Hydrol Process*, 25,
634 4011-4027, 10.1002/hyp.8408, 2011.
- 635 Boos, W. R., and Kuang, Z.: Dominant control of the South Asian monsoon by orographic
636 insulation versus plateau heating, *Nature*, 463, 218-222, 10.1038/nature08707, 2010.
- 637 Bosveld, F. C.: Exchange processes between a coniferous forest and the atmosphere, Ph.D,
638 Wageningen University, 181 pp., 1999.
- 639 Brauman, K., Daily, G., Duarte, T., and Mooney, H.: The nature and value of ecosystem services:
640 An overview highlighting hydrologic services, in: *Annual Review of Environment and*
641 *Resources*, Annual Review of Environment and Resources, Annual Reviews, Palo Alto, 67-98,
642 2007.
- 643 Brutsaert, W.: Aspects of bulk atmospheric boundary layer similarity under free-convective
644 conditions, *Rev. Geophys.*, 37, 439-451, 10.1029/1999rg900013, 1999.
- 645 Cammalleri, C., Anderson, M. C., Ciraolo, G., D'Urso, G., Kustas, W. P., La Loggia, G., and
646 Minacapilli, M.: The impact of in-canopy wind profile formulations on heat flux estimation in an
647 open orchard using the remote sensing-based two-source model, *Hydrol. Earth Syst. Sci.*, 14,
648 2643-2659, 10.5194/hess-14-2643-2010, 2010.
- 649 Chen, F., Mitchell, K., Schaake, J., Xue, Y., Pan, H.-L., Koren, V., Duan, Q. Y., Ek, M., and
650 Betts, A.: Modeling of land surface evaporation by four schemes and comparison with FIFE
651 observations, *Journal of Geophysical Research: Atmospheres*, 101, 7251-7268,
652 10.1029/95jd02165, 1996.
- 653 Chen, J., Jönsson, P., Tamura, M., Gu, Z., Matsushita, B., and Eklundh, L.: A simple method for
654 reconstructing a high-quality NDVI time-series data set based on the Savitzky–Golay filter,
655 *Remote Sensing of Environment*, 91, 332-344, <http://dx.doi.org/10.1016/j.rse.2004.03.014>, 2004.
- 656 Chen, X., Su, Z., Ma, Y., Yang, K., and Wang, B.: Estimation of surface energy fluxes under
657 complex terrain of Mt. Qomolangma over the Tibetan Plateau, *Hydrol. Earth Syst. Sci.*, 17,
658 1607-1618, 10.5194/hess-17-1607-2013, 2013a.
- 659 Chen, X., Su, Z., Ma, Y., Yang, K., Wen, J., and Zhang, Y.: An Improvement of Roughness
660 Height Parameterization of the Surface Energy Balance System (SEBS) over the Tibetan Plateau,
661 *J. Appl. Meteorol. Climatol.*, 52, 607-622, 10.1175/jamc-d-12-056.1, 2013b.
- 662 Chen, Y., Yang, K., He, J., Qin, J., Shi, J., Du, J., and He, Q.: Improving land surface
663 temperature modeling for dry land of China, *J. Geophys. Res.*, 116, D20104,
664 10.1029/2011jd015921, 2011.
- 665 Chen, Y., Yang, K., Qin, J., Zhao, L., Tang, W., and Han, M.: Evaluation of AMSR-E retrievals
666 and GLDAS simulations against observations of a soil moisture network on the central Tibetan
667 Plateau, *Journal of Geophysical Research: Atmospheres*, 118, 4466-4475, 10.1002/jgrd.50301,
668 2013c.
- 669 Coll, C., Wan, Z., and Galve, J. M.: Temperature-based and radiance-based validations of the V5
670 MODIS land surface temperature product, *J. Geophys. Res.*, 114, D20102,
671 10.1029/2009jd012038, 2009.
- 672 Decker, M., Brunke, M. A., Wang, Z., Sakaguchi, K., Zeng, X., and Bosilovich, M. G.:
673 Evaluation of the Reanalysis Products from GSFC, NCEP, and ECMWF Using Flux Tower
674 Observations, *Journal of Climate*, 25, 1916-1944, 10.1175/jcli-d-11-00004.1, 2011.

Formatted: Font: Times New Roman,
12 pt

675 Dee, D. P., Uppala, S. M., Simmons, A. J., Berrisford, P., Poli, P., Kobayashi, S., Andrae, U.,
676 Balmaseda, M. A., Balsamo, G., Bauer, P., Bechtold, P., Beljaars, A. C. M., van de Berg, L.,
677 Bidlot, J., Bormann, N., Delsol, C., Dragani, R., Fuentes, M., Geer, A. J., Haimberger, L., Healy,
678 S. B., Hersbach, H., Hólm, E. V., Isaksen, L., Kållberg, P., Köhler, M., Matricardi, M., McNally,
679 A. P., Monge-Sanz, B. M., Morcrette, J. J., Park, B. K., Peubey, C., de Rosnay, P., Tavolato, C.,
680 Thépaut, J. N., and Vitart, F.: The ERA-Interim reanalysis: configuration and performance of the
681 data assimilation system, *Quarterly Journal of the Royal Meteorological Society*, 137, 553-597,
682 10.1002/qj.828, 2011.

683 Dirmeyer, P. A., Gao, X., Zhao, M., Guo, Z., Oki, T., and Hanasaki, N.: GSWP-2: Multimodel
684 Analysis and Implications for Our Perception of the Land Surface, *Bulletin of the American
685 Meteorological Society*, 87, 1381-1397, 10.1175/bams-87-10-1381, 2006.

686 Fan, L., Liu, S., Bernhofer, C., Liu, H., and Berger, F. H.: Regional land surface energy fluxes by
687 satellite remote sensing in the Upper Xilin River Watershed (Inner Mongolia, China),
688 *Theoretical and Applied Climatology*, 88, 231-245, 10.1007/s00704-006-0241-9, 2007.

689 Fisher, J. B., Tu, K. P., and Baldocchi, D. D.: Global estimates of the land-atmosphere water
690 flux based on monthly AVHRR and ISLSCP-II data, validated at 16 FLUXNET sites, *Remote
691 Sensing of Environment*, 112, 901-919, <http://dx.doi.org/10.1016/j.rse.2007.06.025>, 2008.

692 Flerchinger, G., Xaio, W., Marks, D., Sauer, T., and Yu, Q.: Comparison of algorithms for
693 incoming atmospheric long-wave radiation, *Water Resour. Res.*, 45, W03423,
694 10.1029/2008wr007394, 2009.

695 Gan, T. Y.: Hydroclimatic trends and possible climatic warming in the Canadian Prairies, *Water
696 Resources Research*, 34, 3009-3015, 10.1029/98wr01265, 1998.

697 Goudriaan, J.: Crop micrometeorology: a simulation study, PhD thesis, Wageningen University
698 249 pp., 1977.

699 Guan, X., Huang, J., Guo, N., Bi, J., and Wang, G.: Variability of soil moisture and its
700 relationship with surface albedo and soil thermal parameters over the Loess Plateau, *Advances in
701 Atmospheric Sciences*, 26, 692-700, 10.1007/s00376-009-8198-0, 2009.

702 He, J.: Development of surface meteorological dataset of China with high temporal and spatial
703 resolution, M.S, Inst. of Tibetan Plateau Res., Chin. Acad. of Sci., Beijing, China, 2010.

704 Hogue, T. S., Bastidas, L., Gupta, H., Sorooshian, S., Mitchell, K., and Emmerich, W.:
705 Evaluation and Transferability of the Noah Land Surface Model in Semiarid Environments,
706 *Journal of Hydrometeorology*, 6, 68-84, 10.1175/jhm-402.1, 2005.

707 Hsu, H.-H., and Liu, X.: Relationship between the Tibetan Plateau heating and East Asian
708 summer monsoon rainfall, *Geophys. Res. Lett.*, 30, 2066, 10.1029/2003gl017909, 2003.

709 Huang, J., Zhang, W., Zuo, J., Bi, J., Shi, J., Wang, X., Chang, Z., Huang, Z., Yang, S., Zhang,
710 B., Wang, G., Feng, G., Yuan, J., Zhang, L., Zuo, H., Wang, S., Fu, C., and Jifan, C.: An
711 overview of the semi-arid climate and environment research observatory over the Loess Plateau,
712 *Adv. Atmos. Sci.*, 25, 906-921, 2008.

713 Jia, Z., Liu, S., Xu, Z., Chen, Y., and Zhu, M.: Validation of remotely sensed evapotranspiration
714 over the Hai River Basin, China, *J. Geophys. Res.*, 117, D13113, 10.1029/2011jd017037, 2012.

715 Jiménez, C., Prigent, C., and Aires, F.: Toward an estimation of global land surface heat fluxes
716 from multisatellite observations, *J. Geophys. Res.*, 114, D06305, 10.1029/2008jd011392, 2009.

717 Jiménez, C., Prigent, C., Mueller, B., Seneviratne, S. I., McCabe, M. F., Wood, E. F., Rossow, W.
718 B., Balsamo, G., Betts, A. K., Dirmeyer, P. A., Fisher, J. B., Jung, M., Kanamitsu, M., Reichle,
719 R. H., Reichstein, M., Rodell, M., Sheffield, J., Tu, K., and Wang, K.: Global intercomparison of

720 12 land surface heat flux estimates, *J. Geophys. Res.*, 116, D02102, 10.1029/2010jd014545,
721 2011.

722 Jung, M., Reichstein, M., and Bondeau, A.: Towards global empirical upscaling of FLUXNET
723 eddy covariance observations: validation of a model tree ensemble approach using a biosphere
724 model, *Biogeosciences*, 6, 2001-2013, 10.5194/bg-6-2001-2009, 2009.

725 Jung, M., Reichstein, M., Ciais, P., Seneviratne, S. I., Sheffield, J., Goulden, M. L., Bonan, G.,
726 Cescatti, A., Chen, J., de Jeu, R., Dolman, A. J., Eugster, W., Gerten, D., Gianelle, D., Gobron,
727 N., Heinke, J., Kimball, J., Law, B. E., Montagnani, L., Mu, Q., Mueller, B., Oleson, K., Papale,
728 D., Richardson, A. D., Rouspard, O., Running, S., Tomelleri, E., Viovy, N., Weber, U., Williams,
729 C., Wood, E., Zaehle, S., and Zhang, K.: Recent decline in the global land evapotranspiration
730 trend due to limited moisture supply, *Nature*, 467, 951-954,
731 [http://www.nature.com/nature/journal/v467/n7318/abs/nature09396.html#supplementary-](http://www.nature.com/nature/journal/v467/n7318/abs/nature09396.html#supplementary-information)
732 [information](http://www.nature.com/nature/journal/v467/n7318/abs/nature09396.html#supplementary-information), 2010.

733 Jung, M., Reichstein, M., Margolis, H. A., Cescatti, A., Richardson, A. D., Arain, M. A., Arneith,
734 A., Bernhofer, C., Bonal, D., Chen, J., Gianelle, D., Gobron, N., Kiely, G., Kutsch, W., Lasslop,
735 G., Law, B. E., Lindroth, A., Merbold, L., Montagnani, L., Moors, E. J., Papale, D., Sottocornola,
736 M., Vaccari, F., and Williams, C.: Global patterns of land-atmosphere fluxes of carbon dioxide,
737 latent heat, and sensible heat derived from eddy covariance, satellite, and meteorological
738 observations, *J. Geophys. Res.*, 116, G00J07, 10.1029/2010jg001566, 2011.

739 Kalma, J., McVicar, T., and McCabe, M.: Estimating land surface evaporation: a review of
740 methods using remotely sensed surface temperature data, *Surveys in Geophysics*, 29, 421-469,
741 10.1007/s10712-008-9037-z, 2008.

742 Kalnay, E., Kanamitsu, M., Kistler, R., Collins, W., Deaven, D., Gandin, L., Iredell, M., Saha, S.,
743 White, G., Woollen, J., Zhu, Y., Leetmaa, A., Reynolds, R., Chelliah, M., Ebisuzaki, W.,
744 Higgins, W., Janowiak, J., Mo, K. C., Ropelewski, C., Wang, J., Jenne, R., and Joseph, D.: The
745 NCEP/NCAR 40-year reanalysis project, *Bulletin of the American Meteorological Society*, 77,
746 437-471, 10.1175/1520-0477(1996)077<0437:tnyrp>2.0.co;2, 1996.

747 Lee, E., Barford, C., Kucharik, C., Felzer, B., and Foley, J.: Role of turbulent heat fluxes over
748 land in the monsoon over East Asia, *International Journal of Geosciences*, 2, 420-431,
749 10.4236/ijg.2011.24046., 2011.

750 Lei, H., and Yang, D.: Interannual and seasonal variability in evapotranspiration and energy
751 partitioning over an irrigated cropland in the North China Plain, *Agricultural and Forest*
752 *Meteorology*, 150, 581-589, <http://dx.doi.org/10.1016/j.agrformet.2010.01.022>, 2010a.

753 Lei, H., and Yang, D.: Seasonal and interannual variations in carbon dioxide exchange over a
754 cropland in the North China Plain, *Global Change Biology*, 16, 2944-2957, 10.1111/j.1365-
755 2486.2009.02136.x, 2010b.

756 Li, X., Li, X., Li, Z., Ma, M., Wang, J., Xiao, Q., Liu, Q., Che, T., Chen, E., Yan, G., Hu, Z.,
757 Zhang, L., Chu, R., Su, P., Liu, Q., Liu, S., Wang, J., Niu, Z., Chen, Y., Jin, R., Wang, W., Ran,
758 Y., Xin, X., and Ren, H.: Watershed Allied Telemetry Experimental Research, *Journal of*
759 *Geophysical Research: Atmospheres*, 114, D22103, 10.1029/2008jd011590, 2009.

760 Li, X., Liang, S., Yuan, W., Yu, G., Cheng, X., Chen, Y., Zhao, T., Feng, J., Ma, Z., Ma, M., Liu,
761 S., Chen, J., Shao, C., Li, S., Zhang, X., Zhang, Z., Sun, G., Chen, S., Ohta, T., Varlagin, A.,
762 Miyata, A., Takagi, K., Saiqusa, N., and Kato, T.: Estimation of evapotranspiration over the
763 terrestrial ecosystems in China, *Ecology*, 7, 139-149, 10.1002/eco.1341, 2012a.

764 Li, X., Wang, L., Chen, D., Yang, K., Xue, B., and Sun, L.: Near-surface air temperature lapse
765 rates in the mainland China during 1962–2011, *Journal of Geophysical Research: Atmospheres*,
766 118, 7505-7515, 10.1002/jgrd.50553, 2013.

767 Li, Z., Zheng, F.-L., and Liu, W.-Z.: Spatiotemporal characteristics of reference
768 evapotranspiration during 1961–2009 and its projected changes during 2011–2099 on the Loess
769 Plateau of China, *Agricultural and Forest Meteorology*, 154–155, 147-155,
770 10.1016/j.agrformet.2011.10.019, 2012b.

771 Lin, W., Zhang, L., Du, D., Yang, L., Lin, H., Zhang, Y., and Li, J.: Quantification of land
772 use/land cover changes in Pearl River Delta and its impact on regional climate in summer using
773 numerical modeling, *Reg Environ Change*, 9, 75-82, 10.1007/s10113-008-0057-5, 2009.

774 Liu, J., and Xie, Z.: Improving simulation of soil moisture in China using a multiple
775 meteorological forcing ensemble approach, *Hydrol. Earth Syst. Sci.*, 17, 3355-3369,
776 10.5194/hess-17-3355-2013, 2013.

777 Liu, N., Liu, Q., Wang, L., Liang, S., Wen, J., Qu, Y., and Liu, S.: A statistics-based temporal
778 filter algorithm to map spatiotemporally continuous shortwave albedo from MODIS data, *Hydrol.*
779 *Earth Syst. Sci.*, 17, 10.5194/hess-17-2121-2013, 2013a.

780 Liu, R., Wen, J., Wang, X., Wang, L., Tian, H., Zhang, T. T., Shi, X. K., Zhang, J. H., and Lv, S.
781 N.: Actual daily evapotranspiration estimated from MERIS and AATSR data over the Chinese
782 Loess Plateau, *Hydrol. Earth Syst. Sci.*, 14, 47-58, 10.5194/hess-14-47-2010, 2010.

783 Liu, S., Xu, Z., Wang, W., Jia, Z., Zhu, M., Bai, J., and Wang, J.: A comparison of eddy-
784 covariance and large aperture scintillometer measurements with respect to the energy balance
785 closure problem, *Hydrol. Earth Syst. Sci.*, 15, 1291-1306, 10.5194/hess-15-1291-2011, 2011.

786 Liu, S. M., Xu, Z. W., Zhu, Z. L., Jia, Z. Z., and Zhu, M. J.: Measurements of evapotranspiration
787 from eddy-covariance systems and large aperture scintillometers in the Hai River Basin, China,
788 *Journal of Hydrology*, 487, 24–38, 10.1016/j.jhydrol.2013.02.025,, 2013b.

789 Liu, Y., Zhou, Y., Ju, W., Chen, J., Wang, S., He, H., Wang, H., Guan, D., Zhao, F., Li, Y., and
790 Hao, Y.: Changes of evapotranspiration and water yield in China's terrestrial ecosystems during
791 the period from 2000 to 2010, *Hydrol. Earth Syst. Sci.*, 17, 2121–2129, 10.5194/hessd-10-5397-
792 2013, 2013c.

793 Liu, Z., Zhou, P., Zhang, F., Liu, X., and Chen, G.: Spatiotemporal characteristics of
794 dryness/wetness conditions across Qinghai Province, Northwest China, *Agricultural and Forest*
795 *Meteorology*, 182-183, <http://dx.doi.org/10.1016/j.agrformet.2013.05.013>, 2013d.

796 Ma, L., Zhang, T., Li, Q., Frauenfeld, O. W., and Qin, D.: Evaluation of ERA-40, NCEP-1, and
797 NCEP-2 reanalysis air temperatures with ground-based measurements in China, *J. Geophys. Res.*,
798 113, D15115, 10.1029/2007jd009549, 2008a.

799 Ma, Y., Su, Z., Li, Z., Koike, T., and Menenti, M.: Determination of regional net radiation and
800 soil heat flux over a heterogeneous landscape of the Tibetan Plateau, *Hydrological Processes*, 16,
801 2963-2971, 2002.

802 Ma, Y., Zhong, L., Su, Z., Ishikawa, H., Menenti, M., and Koike, T.: Determination of regional
803 distributions and seasonal variations of land surface heat fluxes from Landsat-7 Enhanced
804 Thematic Mapper data over the central Tibetan Plateau area, *J. Geophys. Res.*, 111, D10305,
805 10.1029/2005jd006742, 2006.

806 Ma, Y., Zhong, L., Wang, B., Ma, W., Chen, X., and Li, M.: Determination of land surface heat
807 fluxes over heterogeneous landscape of the Tibetan Plateau by using the MODIS and in situ data,
808 *Atmos. Chem. Phys.*, 11, 10461-10469, 10.5194/acp-11-10461-2011, 2011.

809 Ma, Y., Kang, S., Zhu, L., Xu, B., Tian, L., and Yao, T.: Tibetan Observation and Research
810 Platform- Atmosphere–land interaction over a heterogeneous landscape, *Bull. Amer. Meteor.*
811 *Soc.*, 89, 1487–1492, 10.1175/2008BAMS2545.1, 2008b.

812 Massman, W. J.: An analytical one-dimensional second-order closure model of turbulence
813 statistics and the lagrangian time scale within and above plant canopies of arbitrary structure,
814 *Boundary Layer Meteorology*, 83, 407-421, 1997.

815 Matthew, O.: Characterization of the effects of climate variation on land surface temperature and
816 soil moisture through stochastic analysis of long term SSM/I observations over the Tibetan
817 plateau, Master, International Institute for Geo-information Science and Earth Observation,
818 University of Twente, Enschede, The Netherlands, 1-67 pp., 2010.

819 Meir, P., and Woodward, F. I.: Amazonian rain forests and drought: response and vulnerability,
820 *New Phytologist*, 187, 553-557, 10.1111/j.1469-8137.2010.03390.x, 2010.

821 Mi, N., Yu, G. R., Wang, P. X., Wen, X. F., and Sun, X. M.: A preliminary study for spatial
822 representiveness of flux observation at ChinaFLUX sites, *Science in China Series D-Earth*
823 *Sciences*, 49, 24-35, 10.1007/s11430-006-8024-9|ISSN 1006-9313, 2006.

824 Moody, E. G., King, M. D., Platnick, S., Schaaf, C. B., and Feng, G.: Spatially complete global
825 spectral surface albedos: value-added datasets derived from Terra MODIS land products,
826 *Geoscience and Remote Sensing, IEEE Transactions on*, 43, 144-158, 10.1109/tgrs.2004.838359,
827 2005.

828 Mu, Q., Heinsch, F. A., Zhao, M., and Running, S. W.: Development of a global
829 evapotranspiration algorithm based on MODIS and global meteorology data, *Remote Sensing of*
830 *Environment*, 111, 519-536, 10.1016/j.rse.2007.04.015, 2007.

831 Mueller, B., Seneviratne, S. I., Jimenez, C., Corti, T., Hirschi, M., Balsamo, G., Ciais, P.,
832 Dirmeyer, P., Fisher, J. B., Guo, Z., Jung, M., Maignan, F., McCabe, M. F., Reichle, R.,
833 Reichstein, M., Rodell, M., Sheffield, J., Teuling, A. J., Wang, K., Wood, E. F., and Zhang, Y.:
834 Evaluation of global observations-based evapotranspiration datasets and IPCC AR4 simulations,
835 *Geophys. Res. Lett.*, 38, L06402, 10.1029/2010gl046230, 2011.

836 Muller, J.-P., López, G., Watson, G., Shane, N., Kennedy, T., Yuen, P., Lewis, P., Fischer, J.,
837 Guanter, L., Domench, C., Preusker, R., North, P., Heckel, A., Danne, O., and Krämer, U.: The
838 ESA GlobAlbedo Project for mapping the Earth's land surface albedo for 15 Years from
839 European Sensors., , *IEEE Geoscience and Remote Sensing Symposium (IGARSS)* , IEEE, ,
840 Munich, Germany, , 2012.

841 Norman, J. M., Anderson, M. C., Kustas, W. P., French, A. N., Mecikalski, J., Torn, R., Diak, G.
842 R., Schmugge, T. J., and Tanner, B. C. W.: Remote sensing of surface energy fluxes at 101-m
843 pixel resolutions, *Water Resources Research*, 39, 1221, 10.1029/2002wr001775, 2003.

844 Piao, S., Mohammat, A., Fang, J., Cai, Q., and Feng, J.: NDVI-based increase in growth of
845 temperate grasslands and its responses to climate changes in China, *Global Environmental*
846 *Change*, 16, 340-348, <http://dx.doi.org/10.1016/j.gloenvcha.2006.02.002>, 2006.

847 Qiu, J.: Monsoon Melee, *Science*, 340, 1400-1401, 10.1126/science.340.6139.1400, 2013.

848 Rienecker, M. M., Suarez, M. J., Gelaro, R., Todling, R., Bacmeister, J., Liu, E., Bosilovich, M.
849 G., Schubert, S. D., Takacs, L., Kim, G.-K., Bloom, S., Chen, J., Collins, D., Conaty, A., da
850 Silva, A., Gu, W., Joiner, J., Koster, R. D., Lucchesi, R., Molod, A., Owens, T., Pawson, S.,
851 Pegion, P., Redder, C. R., Reichle, R., Robertson, F. R., Ruddick, A. G., Sienkiewicz, M., and
852 Woollen, J.: MERRA: NASA's Modern-Era Retrospective Analysis for Research and
853 Applications, *Journal of Climate*, 24, 3624-3648, 10.1175/jcli-d-11-00015.1, 2011.

854 Riihel, A., Manninen, T., Laine, V., Andersson, K., and Kaspar, F.: CLARA-SAL: a global 28-yr
855 timeseries of Earth's black-sky surface albedo, *Atmos. Chem. Phys.*, 13, 3743-3762,
856 10.5194/acp-13-3743-2013, 2013.

857 Roads, J., and Betts, A.: NCEP-NCAR and ECMWF reanalysis surface water and energy
858 budgets for the Mississippi River Basin, *Journal of Hydrometeorology*, 1, 88-94, 10.1175/1525-
859 7541(2000)001<0088:nnaers>2.0.co;2, 2000.

860 Rodell, M., Houser, P. R., Jambor, U., Gottschalck, J., Mitchell, K., Meng, C. J., Arsenault, K.,
861 Cosgrove, B., Radakovich, J., Bosilovich, M., Entin, J. K., Walker, J. P., Lohmann, D., and Toll,
862 D.: The Global Land Data Assimilation System, *Bulletin of the American Meteorological*
863 *Society*, 85, 381-394, 10.1175/bams-85-3-381, 2004.

864 Ryu, Y., Baldocchi, D. D., Kobayashi, H., van Ingen, C., Li, J., Black, T. A., Beringer, J., van
865 Gorsel, E., Knohl, A., Law, B. E., and Rouspard, O.: Integration of MODIS land and atmosphere
866 products with a coupled-process model to estimate gross primary productivity and
867 evapotranspiration from 1 km to global scales, *Global Biogeochemical Cycles*, 25, GB4017,
868 10.1029/2011gb004053, 2011.

869 Ryu, Y., Baldocchi, D. D., Black, T. A., Detto, M., Law, B. E., Leuning, R., Miyata, A.,
870 Reichstein, M., Vargas, R., Ammann, C., Beringer, J., Flanagan, L. B., Gu, L., Hutley, L. B.,
871 Kim, J., McCaughey, H., Moors, E. J., Rambal, S., and Vesala, T.: On the temporal upscaling of
872 evapotranspiration from instantaneous remote sensing measurements to 8-day mean daily-sums,
873 *Agricultural and Forest Meteorology*, 152, 212-222,
874 <http://dx.doi.org/10.1016/j.agrformet.2011.09.010>, 2012.

875 Salama, M. S., Velde, R., Zhong, L., Ma, Y., Ofwono, M., and Su, Z.: Decadal variations of land
876 surface temperature anomalies observed over the Tibetan Plateau by the Special Sensor
877 Microwave Imager (SSM/I) from 1987 to 2008, *Climatic Change*, 114, 769-781,
878 10.1007/s10584-012-0427-3, 2012.

879 Scherler, D., Bookhagen, B., and Strecker, M. R.: Spatially variable response of Himalayan
880 glaciers to climate change affected by debris cover, *Nature Geosci*, 4, 156-159,
881 <http://www.nature.com/ngeo/journal/v4/n3/abs/ngeo1068.html#supplementary-information>,
882 2011.

883 Sheffield, J., Goteti, G., and Wood, E. F.: Development of a 50-Year high-resolution global
884 dataset of meteorological forcings for land surface modeling, *Journal of Climate*, 19, 3088-3111,
885 10.1175/jcli3790.1, 2006.

886 Shu, Y., Stisen, S., Jensen, K. H., and Sandholt, I.: Estimation of regional evapotranspiration
887 over the North China Plain using geostationary satellite data, *International Journal of Applied*
888 *Earth Observation and Geoinformation*, 13, 192-206, 10.1016/j.jag.2010.11.002, 2011.

889 Simard, M., Pinto, N., Fisher, J. B., and Baccini, A.: Mapping forest canopy height globally with
890 spaceborne lidar, *J. Geophys. Res.*, 116, G04021, 10.1029/2011jg001708, 2011.

891 Su, Z., Schmugge, T., Kustas, W. P., and Massman, W. J.: An evaluation of two models for
892 estimation of the roughness height for heat transfer between the land surface and the atmosphere,
893 *Journal of Applied Meteorology*, 40, 1933-1951, 2001.

894 Su, Z.: The Surface Energy Balance System(SEBS) for estimation of turbulent heat fluxes,
895 *Hydrology and Earth System Sciences*, 6, 85-99, 2002.

896 Su, Z., de Rosnay, P., Wen, J., Wang, L., and Zeng, Y.: Evaluation of ECMWF's soil moisture
897 analyses using observations on the Tibetan Plateau, *Journal of Geophysical Research:*
898 *Atmospheres*, 118, 5304-5318, 10.1002/jgrd.50468, 2013.

899 Suh, M.-S., and Lee, D.-K.: Impacts of land use/cover changes on surface climate over east Asia
900 for extreme climate cases using RegCM2, *Journal of Geophysical Research: Atmospheres*, 109,
901 D02108, 10.1029/2003jd003681, 2004.
902 Sun, L., and Wu, G.: Influence of land evapotranspiration on climate variations, *Science in China*
903 *Series D: Earth Sciences*, 44, 838-846, 10.1007/bf02907096, 2001.
904 Tang, W. J., Yang, K., Qin, J., Cheng, C. C. K., and He, J.: Solar radiation trend across China in
905 recent decades: a revisit with quality-controlled data, *Atmos. Chem. Phys.*, 11, 393-406,
906 10.5194/acp-11-393-2011, 2011.
907 Taniguchi, K., and Koike, T.: Seasonal variation of cloud activity and atmospheric profiles over
908 the eastern part of the Tibetan Plateau, *J. Geophys. Res.-Atmos.*, 113, 10104-10104, 2008.
909 Timmermans, J.: Coupling optical and thermal directional radiative transfer to biophysical
910 processes in vegetated canopies, Phd, faculty of geo-information science and earth observation,
911 University of Twente, Enschede, The Netherlands, 1-157 pp., 2011.
912 Vinukollu, R. K., Meynadier, R., Sheffield, J., and Wood, E. F.: Multi-model, multi-sensor
913 estimates of global evapotranspiration: climatology, uncertainties and trends, *Hydrol Process*, 25,
914 3993-4010, 10.1002/hyp.8393, 2011a.
915 Vinukollu, R. K., Wood, E. F., Ferguson, C. R., and Fisher, J. B.: Global estimates of
916 evapotranspiration for climate studies using multi-sensor remote sensing data: Evaluation of
917 three process-based approaches, *Remote Sensing of Environment*, 115, 801-823,
918 10.1016/j.rse.2010.11.006, 2011b.
919 Wan, Z., and Li, Z. L.: Radiance - based validation of the V5 MODIS land - surface temperature
920 product, *International Journal of Remote Sensing*, 29, 5373-5395, 10.1080/01431160802036565,
921 2008.
922 Collection-5 MODIS land surface temperature products users' guide.
923 <http://www.ices.ucsb.edu/modis/LstUsrGuide/usrguide.html>, 2009.
924 Wang, A., and Zeng, X.: Evaluation of multireanalysis products with in situ observations over
925 the Tibetan Plateau, *J. Geophys. Res.*, 117, D05102, 10.1029/2011jd016553, 2012.
926 Wang, A., Barlage, M., Zeng, X., and Draper, C. S.: Comparison of land skin temperature from a
927 land model, remote sensing, and in-situ measurement, *Journal of Geophysical Research:*
928 *Atmospheres*, 2013JD021026, 10.1002/2013jd021026, 2014.
929 Wang, G., Huang, J., Guo, W., Zuo, J., Wang, J., Bi, J., Huang, Z., and Shi, J.: Observation
930 analysis of land-atmosphere interactions over the Loess Plateau of northwest China, *J. Geophys.*
931 *Res.*, 115, D00K17, 10.1029/2009jd013372, 2010.
932 Wang, K., Wang, P., Li, Z., Cribb, M., and Sparrow, M.: A simple method to estimate actual
933 evapotranspiration from a combination of net radiation, vegetation index, and temperature,
934 *Journal of Geophysical Research: Atmospheres*, 112, D15107, 10.1029/2006jd008351, 2007.
935 Wang, K., and Liang, S.: An improved method for estimating global evapotranspiration based on
936 satellite determination of surface net radiation, vegetation index, temperature, and soil moisture,
937 *Journal of Hydrometeorology*, 9, 712-727, 10.1175/2007jhm911.1, 2008.
938 Wang, S., Zhang, Y., Lv, S., Liu, H., and Shang, L.: Estimation of turbulent fluxes using the
939 flux-variance method over alpine meadows surface in eastern Tibetan Plateau, *Advances in*
940 *Atmospheric Sciences*, 30, 411-424, 10.1007/s00376-012-2056-1, 2013.
941 Wu, G., Liu, Y., He, B., Bao, Q., Duan, A., and Jin, F.-F.: Thermal controls on the Asian
942 summer monsoon, *Sci. Rep.*, 2, 404, 10.1038/srep00404 (2012), 2012.

Formatted: Font: (Default) Cambria Math, 12 pt

Formatted: Font: Times New Roman, 12 pt

Formatted: Font: (Default) Cambria Math, 12 pt

Formatted: Font: Times New Roman, 12 pt

943 Yan, H., Wang, S. Q., Billesbach, D., Oechel, W., Zhang, J. H., Meyers, T., Martin, T. A.,
944 Matamala, R., Baldocchi, D., Bohrer, G., Dragoni, D., and Scott, R.: Global estimation of
945 evapotranspiration using a leaf area index-based surface energy and water balance model,
946 *Remote Sensing of Environment*, 124, 581-595, 10.1016/j.rse.2012.06.004, 2012.

947 Yang, K., Koike, T., Fujii, H., Tamagawa, K., and Hirose, N.: Improvement of surface flux
948 parametrizations with a turbulence-related length, *Quarterly Journal of the Royal Meteorological
949 Society*, 128, 2073-2087, 2002.

950 Yang, K., Ding, B., Qin, J., Tang, W., Lu, N., and Lin, C.: Can aerosol loading explain the solar
951 dimming over the Tibetan Plateau?, *Geophys. Res. Lett.*, 39, L20710, 10.1029/2012gl053733,
952 2012.

953 Yao, T., Wang, Y., Liu, S., Pu, J., Shen, Y., and Lu, A.: Recent glacial retreat in High Asia in
954 China and its impact on water resource in Northwest China, *Science in China Series D: Earth
955 Sciences*, 47, 1065-1075, 10.1360/03yd0256, 2004.

956 Yao, Y., Liang, S., Cheng, J., Liu, S., Fisher, J. B., Zhang, X., Jia, K., Zhao, X., Qin, Q., Zhao,
957 B., Han, S., Zhou, G., Zhou, G., Li, Y., and Zhao, S.: MODIS-driven estimation of terrestrial
958 latent heat flux in China based on a modified Priestley–Taylor algorithm, *Agricultural and Forest
959 Meteorology*, 171–172, 187-202, <http://dx.doi.org/10.1016/j.agrformet.2012.11.016>, 2013.

960 Yu, G.-R., Wen, X.-F., Sun, X.-M., Tanner, B. D., Lee, X., and Chen, J.-Y.: Overview of
961 ChinaFLUX and evaluation of its eddy covariance measurement, *Agricultural and Forest
962 Meteorology*, 137, 125-137, <http://dx.doi.org/10.1016/j.agrformet.2006.02.011>, 2006.

963 Yuan, W., Liu, S., Yu, G., Bonnefond, J.-M., Chen, J., Davis, K., Desai, A. R., Goldstein, A. H.,
964 Gianelle, D., Rossi, F., Suyker, A. E., and Verma, S. B.: Global estimates of evapotranspiration
965 and gross primary production based on MODIS and global meteorology data, *Remote Sensing of
966 Environment*, 114, 1416-1431, <http://dx.doi.org/10.1016/j.rse.2010.01.022>, 2010.

967 Zhang, C., Chen, F., Miao, S., Li, Q., Xia, X., and Xuan, C.: Impacts of urban expansion and
968 future green planting on summer precipitation in the Beijing metropolitan area, *Journal of
969 Geophysical Research: Atmospheres*, 114, D02116, 10.1029/2008jd010328, 2009a.

970 Zhang, K., Kimball, J. S., Nemani, R. R., and Running, S. W.: A continuous satellite-derived
971 global record of land surface evapotranspiration from 1983 to 2006, *Water Resources Research*,
972 46, W09522, 10.1029/2009wr008800, 2010.

973 Zhang, L., Li, Y., Li, Y., and Zhao, X.: Seasonal changes of turbulent fluxes at a typical
974 agricultural site in the Chengdu Plain based on quality-controlled data, *Journal of the
975 Meteorological Society of Japan. Ser. II*, 90C, 195-202, 2012.

976 Zhang, X., Ren, Y., Yin, Z.-Y., Lin, Z., and Zheng, D.: Spatial and temporal variation patterns of
977 reference evapotranspiration across the Qinghai-Tibetan Plateau during 1971&-2004, *J. Geophys.
978 Res.*, 114, D15105, 10.1029/2009jd011753, 2009b.

979 Zhao, B., Yan, Y., Guo, H., He, M., Gu, Y., and Li, B.: Monitoring rapid vegetation succession
980 in estuarine wetland using time series MODIS-based indicators: An application in the Yangtze
981 River Delta area, *Ecological Indicators*, 9, 346-356,
982 <http://dx.doi.org/10.1016/j.ecolind.2008.05.009>, 2009.

983 Zhong, L., Su, Z., Ma, Y., Salama, M. S., and Sobrino, J. A.: Accelerated changes of
984 environmental conditions on the Tibetan Plateau caused by climate change, *Journal of Climate*,
985 24, 6540-6550, 10.1175/jcli-d-10-05000.1, 2011.

986 | Zhou, L., and Huang, R.: Interdecadal variability of sensible heat flux in arid and semi-arid
987 | region of Northwest China and its relationship to summer precipitation in China (in Chinese),
988 | Chinese J. Atmos. Sci., 32, 1276-1288, 2008.
989 | Zhou, L., and Huang, R.: An assessment of the quality of surface sensible heat flux derived from
990 | reanalysis data through comparison with station observations in Northwest China, Advances in
991 | Atmospheric Sciences, 27, 500-512, 10.1007/s00376-009-9081-8, 2010.
992 | Zhu, X., Liu, Y., and Wu, G.: An assessment of summer sensible heat flux on the Tibetan
993 | Plateau from eight data sets, Science China Earth Sciences, 55, 779-786, 10.1007/s11430-012-
994 | 4379-2, 2012.

995

996

997

998

999

1000

1001

1002

1003

1004

1005

1006

1007

1008

1009 Table 1. Input datasets used for calculating land surface fluxes for China (see Sections 2 and 3
 1010 for an explanation of abbreviations)

Variables	Data source	Temporal resolution	Availability	Domain	Spatial resolution (degrees)	Method
SWD	ITPCAS	3 hours	1979-2010	China land	0.1	Reanalysis
SWU	ITPCAS& GlobAlbedo	3 hours	1982-2009	China land	0.1	Satellite&Reanalysis
LWD	ITPCAS	3 hours	1979-2010	China land	0.1	Reanalysis
LWU	MOD11C3&MYD11C3 V5&Emis of Chen et al. 2013	1 month	2000-2012	China land	0.05	Satellite
Ta	ITPCAS	3 hours	1979-2010	China land	0.1	Reanalysis
Q	ITPCAS	3 hours	1979-2010	China land	0.1	Reanalysis
Ws	ITPCAS	3 hours	1979-2010	China land	0.1	Reanalysis
P	ITPCAS	3 hours	1979-2010	China land	0.1	Reanalysis
LST	MOD11C3 V5&MYD11C3 V5	1 month	2000-2012	Global	0.05	Satellite
h_c	GLAS&SPOT VEGETATION	1 month	2000-2012	China land	0.01	Satellite
A	GlobAlbedo	1 month	2000-2010	Global	0.05	Satellite
NDVI	SPOT VEGETATION	10 days	1998-2012	Global	0.01	Satellite
LAI	MOD15A2&MCD15A2	8 days	Feb, 2000-Jul, 2002 Aug, 2002-2012/	Global	0.01	Satellite

1011

1012

1013

1014

1015

1016

1017

Table 2. Flux tower sites supplying measurement data for product validation

	Lat[deg]/ Lon[deg]	Land cover	Eddy covariance	Radiometer	Measurement period	Site elevation (m)	Reference
WJ	30.4200N/ 103.5000E	Crop	CSAT3,Licor7500 (10 HZ)	CNR-1	Mar 2008 - Aug 2009	539	Zhang et al. (2012)
MQ	33.8872N/ 102.1406E	Alpine meadow	CSAT3,Licor7500 (10 HZ)	CNR-1	Apr 2009 - May 2010	3439	Wang et al. (2013)
AL	33.3905N/ 79.7035E	Bare soil	CSAT3,Licor7500 (10 HZ)	CNR-1	Jul 2010 - Dec 2010	4700	Ma et al. (2008b)
BJ	31.3686N/ 91.8986E	Alpine grass	CSAT3,Licor7500 (10 HZ)	CNR-1	Jan 2008 - Dec 2010	4520	Ma et al. (2011)
MY	40.6038N/ 117.3233E	Orchard	CSAT3,Licor7500 (10 HZ)	CNR-1	Jan 2008 - Dec 2010	350	Liu et al. (2013b)
DX	39.6213N/ 116.4270E	Crop	CSAT3,Licor7500 (10 HZ)	CNR-1	Jan 2008 - Dec 2010	100	Liu et al. (2013b)
GT	36.5150N/ 115.1274E	Crop	CSAT3,Licor7500 (10 HZ)	CNR-1	Jan 2008 - Dec 2010	30	Liu et al. (2013b)
YC	36.9500N/ 116.600E	Crop	CSAT3,Licor7500 (10 HZ)	CNR-1	Oct 2002 - Oct 2004	13	Flerchinger et al. (2009)
DT	31.5169N/ 121.9717E	Wetland	CSAT3,Licor7500 (10 HZ)	CNR-1	Jan 2005 - Dec 2007	5	Zhao et al. (2009)
SC	35.95N/ 104.133E	Dry land	CSAT3,Licor7500 (10 HZ)	CNR-1	Jan 2007 - Dec 2008	1965	Huang et al. (2008)
WS	36.6488N/ 116.0543E	Winter wheat / summer maize	CSAT3,Licor7500 (10 HZ)	CNR-1	Jan 2006 - Dec 2008	30	Lei and Yang (2010a)

1018

1019

1020

1021

1022

1023

1024

1025

1026

1027

1028

1029

1030

Table 3. Comparison of accuracy of our flux data product and GLDAS against in-situ measurements from 11 Chinese flux towers. MB is mean of observation minus model simulation.

		Energy flux					Radiation flux				
		H (Wm ⁻²)	LE (Wm ⁻²)	G0 (Wm ⁻²)	Rn (Wm ⁻²)	Mean	SWD (Wm ⁻²)	SWU (Wm ⁻²)	LWD (Wm ⁻²)	LWU (Wm ⁻²)	Mean
Our flux data product	Slope	0.39	0.9	0.87	0.92	0.77	0.95	0.68	0.91	0.95	0.87
	Intercept	-0.5	-6.1	6.1	-20.2	-8.2	13.6	10.9	-0.66	16.6	9.9
	RMSE	21.5	21.9	11.7	36.2	22.8	28.3	10.2	32.8	9.6	20.2
	MB	14.7	10.1	-5.7	26.3	11.4	-5.7	-0.65	28.9	2.4	6.2
	R	0.41	0.85	0.50	0.86	0.66	0.89	0.78	0.98	0.99	0.91
	Sample	280	284	197	313	270	310	307	307	307	308
GLDAS	Slope	0.77	0.87	0.58	1.0	0.81	0.99	0.75	0.87	1.0	0.90
	Intercept	20.83	5.1	-1.34	8.0	8.2	34.9	13.1	27.7	-4.5	17.8
	RMSE	26.6	20.6	6.7	17.9	17.9	45.6	15.9	19.2	11.1	23.0
	MB	-15.8	0.75	3.0	-10.4	-5.6	-32.87	-4.6	13.5	-3.2	-6.8
	R	0.46	0.80	0.61	0.95	0.71	0.87	0.65	0.99	0.98	0.87
	Sample	249	250	162	281	236	275	272	272	275	274

1031

1032

1033

1034

1035

1036

1037

1038

1039

1040

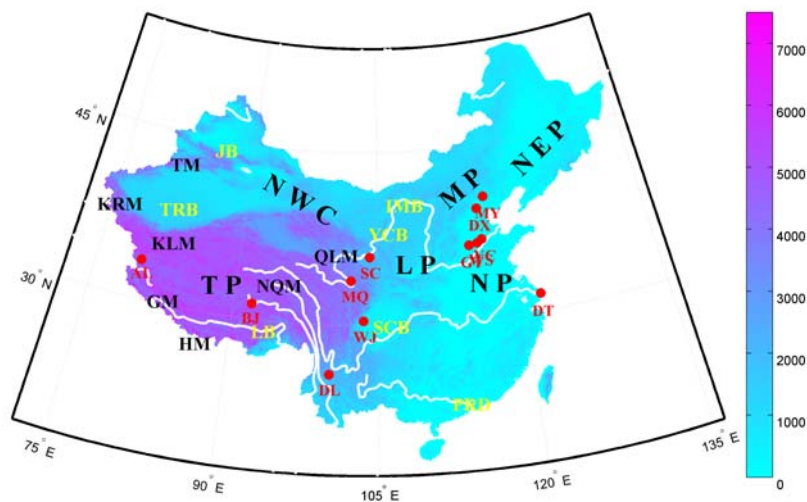
1041

1042
 1043
 1044
 1045
 1046
 1047

Table 4. Comparison of statistical values reported in similar studies

Reference	Research area	Method	Statistical parameters	H (Wm ⁻²)	LE (Wm ⁻²)	Flux network	Note
This study	Chinese landmass	SEBS	RMSE	23.1	21.9	flux towers in China	
			MB	16.8	8.3		
			R	0.6	0.8		
Wang et al. 2007	Southern Great Plains, USA	Regression method	RMSE	×	29.8	flux towers in Southern Great Plains, USA	calculated from Table 9
			MB	×	12.17		
			R	×	0.91		
Jiménez et al. 2009	global	Statistical method	RMSE	×	×	AmeriFlux	calculated from Tables 5 and 7
			MB	-5.23	7.9		
			R	0.68	0.76		
Vinukollu et al. 2011b	global	SEBS	RMSE	40.5	26.1	AmeriFlux	calculated from Table 4
			MB	27.98	-7.74		
			R	0.53	0.51		

1048
 1049
 1050



1051

1052

1053 | Figure 1. A DEM-NDVI map of the Chinese landmass based on SPOT satellite data. The symbols
 1054 indicate major physical phenomena: Tibetan Plateau (TP), northwestern China (NWC), inner
 1055 Mongolian Plateau (MP), Loess Plateau (LP), North China Plain (NP), northeastern China Plain
 1056 (NEP); Pearl River delta (PRD), Sichuan (SCB), Yinchuan (YCB), the inner Mongolian (IMB),
 1057 and Lhasa (LB), Tarim (TRB), Junggar (JB) basins; the Himalaya (HM), Ganges (GM),
 1058 Kunlun (KL), Karakorum (KRM), Tianshan (TM), Nyainqentanglha (NQM) and Qilian
 1059 mountain (QLM) ranges. The plateau and plain letter symbols are in red type. The basins letter
 1060 symbols are in green type. The flux station letter symbols are in yellow type. Blue lines
 1061 show several of the major rivers in China. Black lines indicate the borders of provinces.

1062

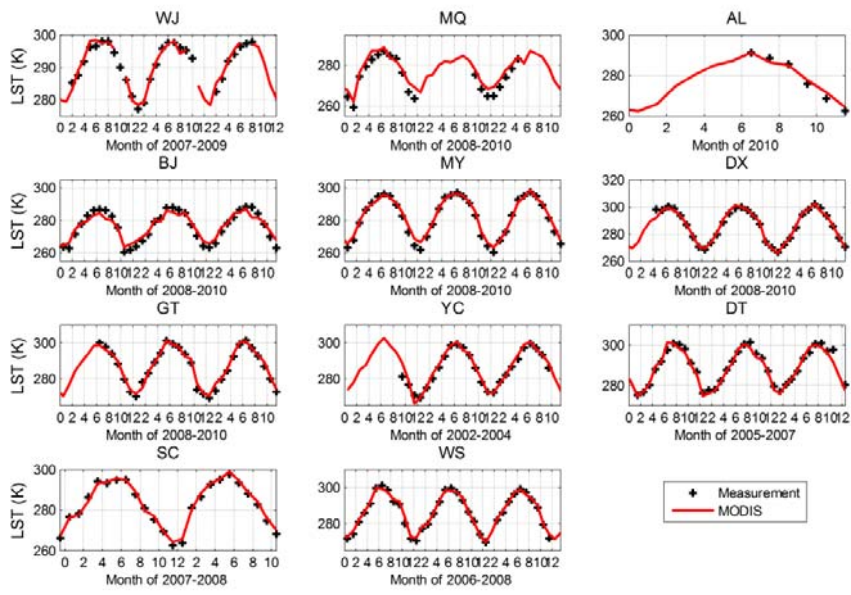
1063

1064

1065

1066

1067



Formatted: Font: Times New Roman, 12 pt

1068
1069
1070
1071
1072

Fig. 2 Time series comparison of monthly averaged LST derived from MOD11C3&MYD11C3 and in-situ measurements.

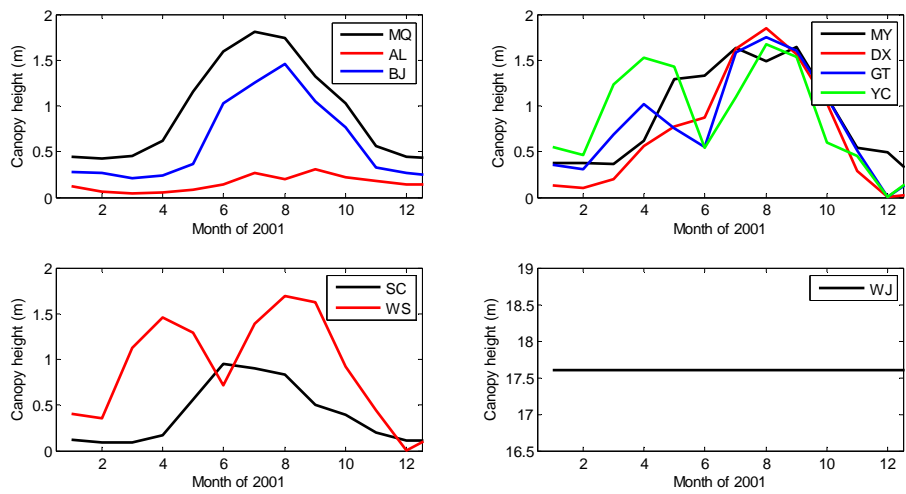


Fig. 3 Monthly variation of canopy height at the 10 flux stations

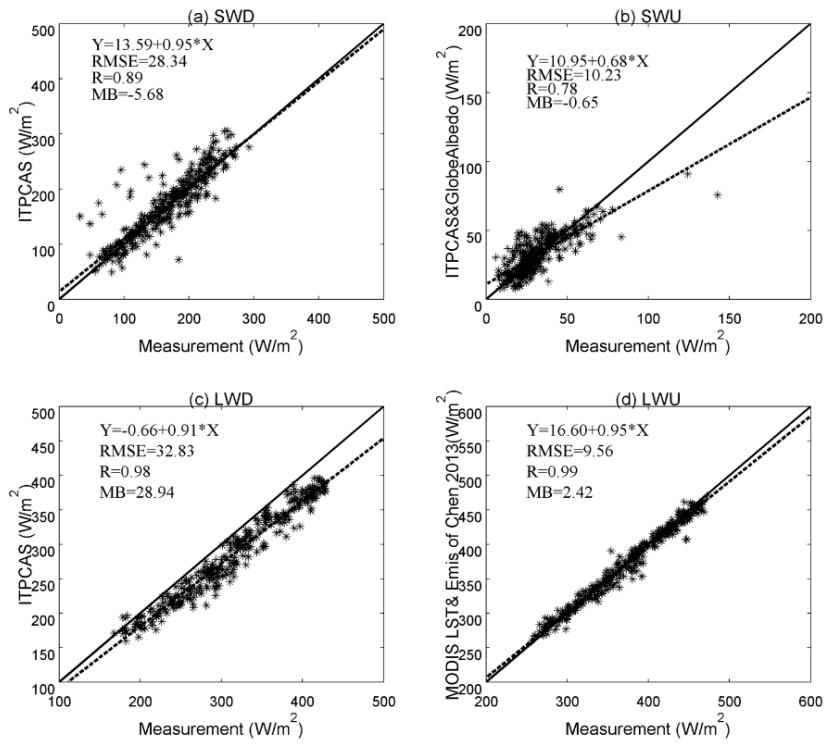
Formatted: Font: Times New Roman, 12 pt

Formatted: Centered

Formatted: Space After: 0 pt, Line spacing: Double

1073
1074
1075
1076
1077
1078
1079
1080
1081

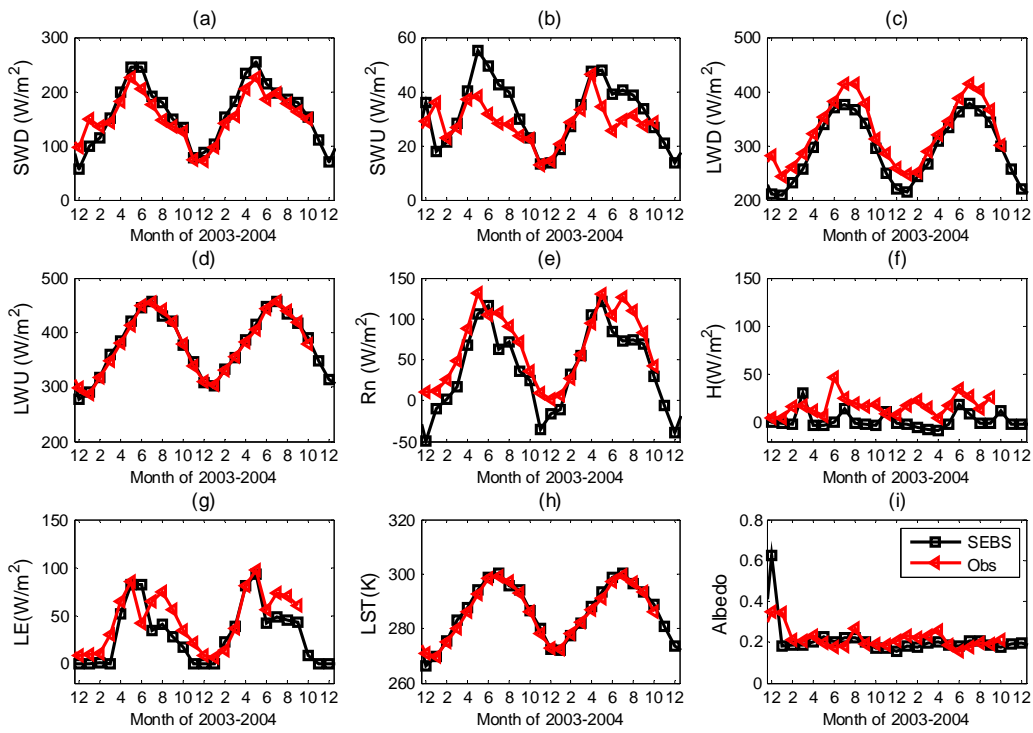
Formatted: Font: Times New Roman, 12 pt



1082

1083
1084

Figure 4 Scatter point for downward shortwave (SWD), upward shortwave (SWU), downward longwave (LWD), and upward longwave (LWU) radiation against in-situ measurement.



1085 | Figure 52. Time-series comparison of SEBS input and output variables against measurements at
 1086 Yucheng station. Black lines are SEBS results; red lines are measured values.

1087

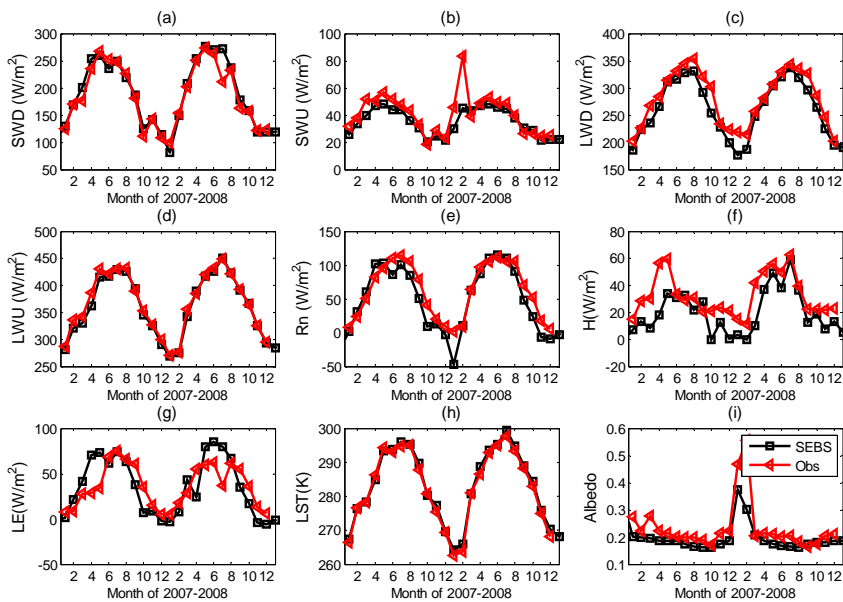
1088

1089

1090

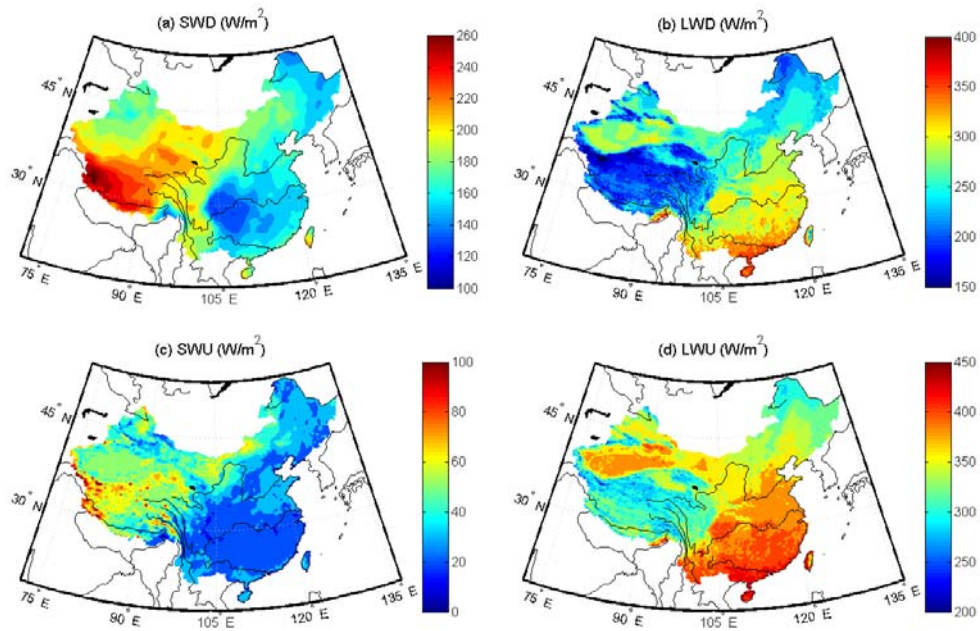
1091

1092



1093

1094 | Figure 63. Time-series comparison of SEBS input and output variables against measurements at
 1095 SC station. Black lines are SEBS results; red lines are measured values.



1096

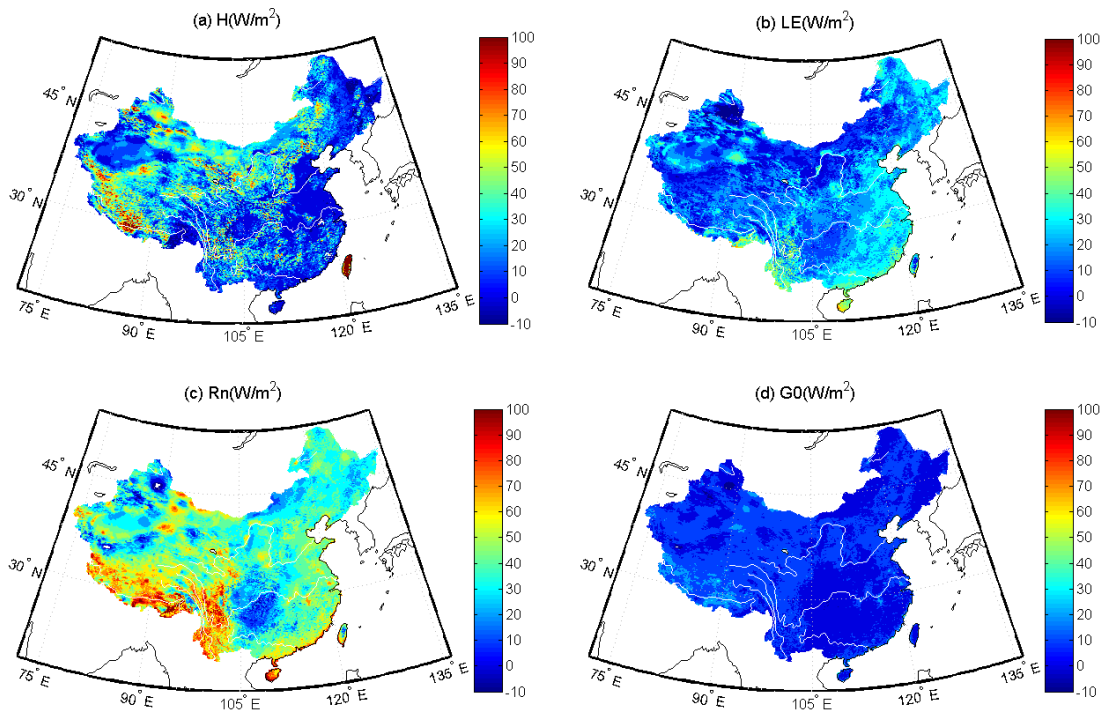
1097

1098

1099

1100 | Figure 74. Maps of annual average (a) downward short-wave radiation (SWD), (b) downward
 1101 long-wave radiation (LWD), (c) upward short-wave radiation (SWU), and (d) upward long-wave
 1102 radiation (LWU) from 2001 to 2010. Black lines show several major rivers in China.

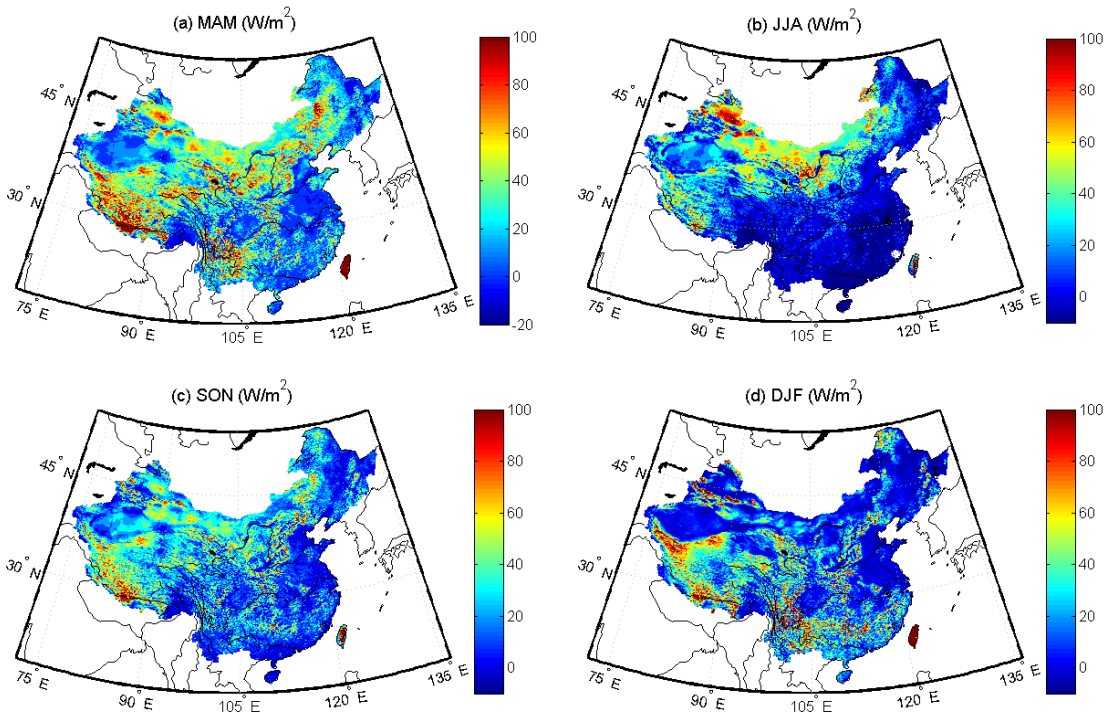
1103



1104

1105 | Figure 85. Maps of multiyear (2001–2010) means of retrieved fluxes: (a) sensible heat flux (H),
 1106 (b) latent heat flux (LE), (c) net radiation (Rn), and (d) ground heat flux (G0). White lines show
 1107 several major rivers in China.

1108

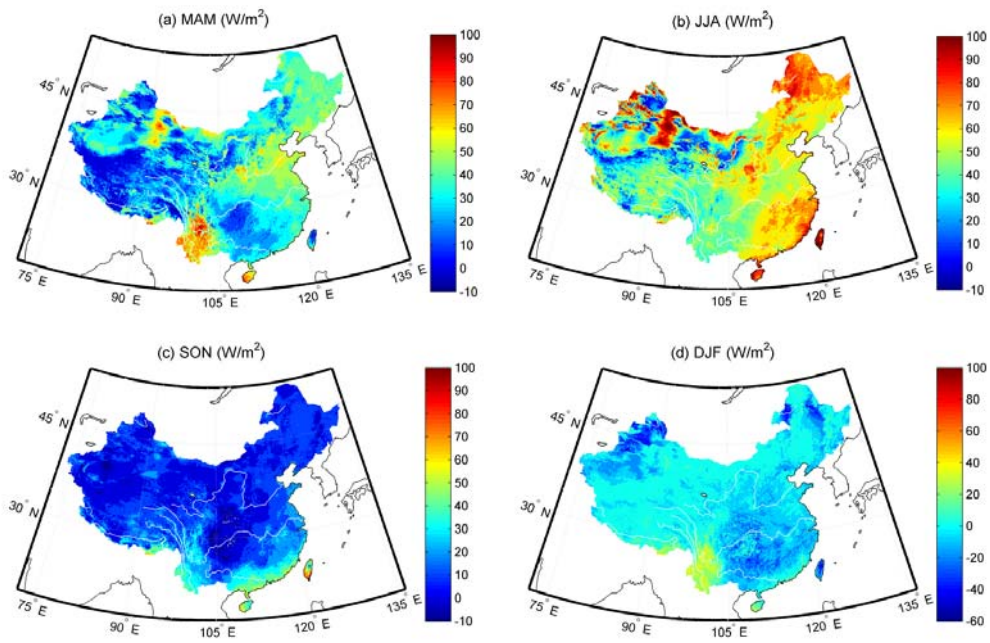


1109 | Figure 96. Maps of seasonal average sensible heat flux for (a) March-May (MAM), (b) June-
 1110 August (JJA), (c) September-November (SON), and (d) December- February (DJF) from 2001 to
 1111 2010. Black lines show several major rivers in China.

1112

1113

1114



1115

1116

1117 | Figure 107. Maps of seasonal average latent heat flux for (a) March-May (MAM), (b) June-
 1118 August (JJA), (c) September-November (SON), and (d) December- February (DJF) from 2001 to
 1119 2010. White lines show several major rivers in China.

1120

1121

1122

1123

1124

1125

1126

1127

1128

1129

1130

1131

1132

1133

1134

1135

1136

1137

1138

1139

1140

1141

1142

1143

1144

1145

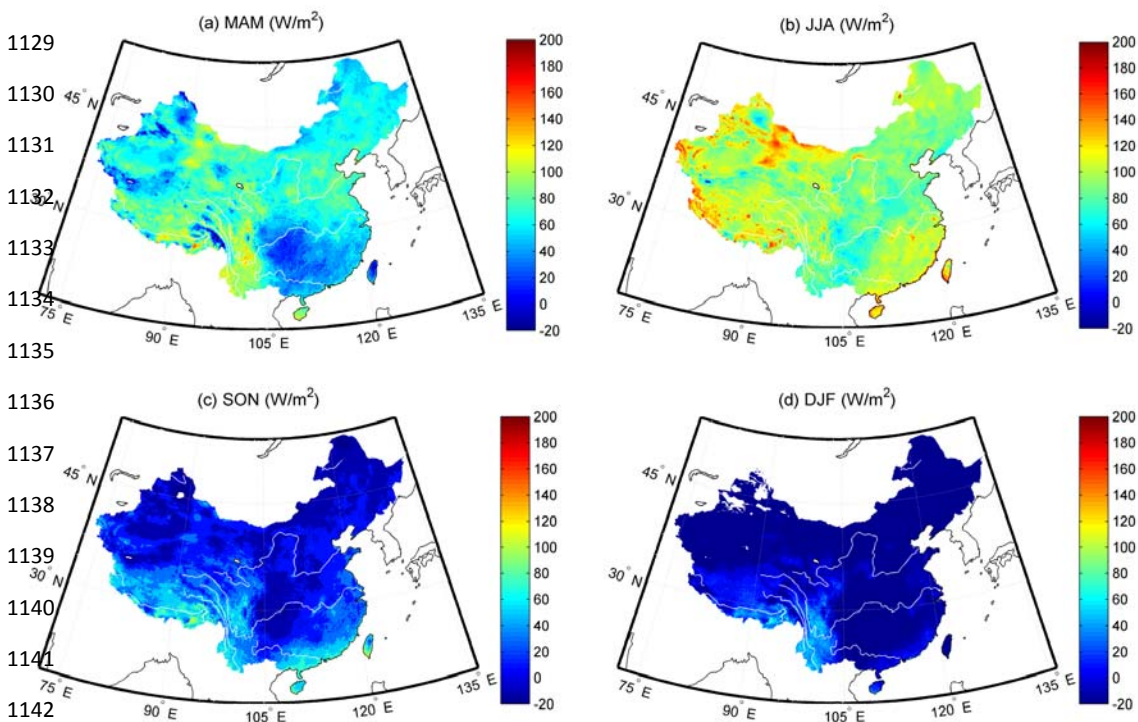
1146

1148

1149

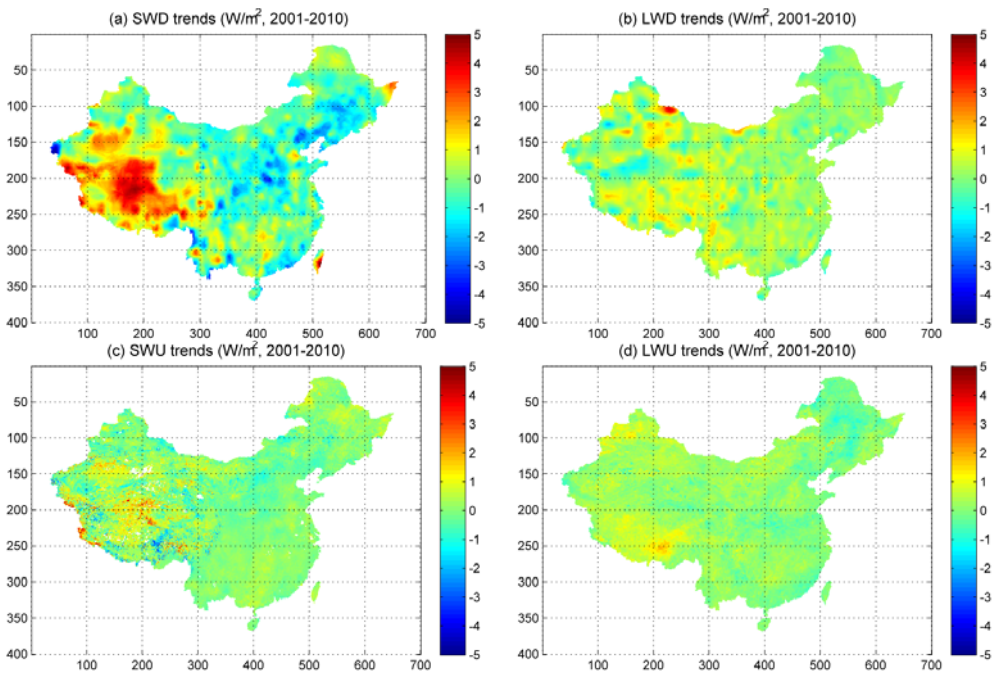
1150

1151



1145 | Figure 118. Maps of seasonal average net radiation for (a) March-May (MAM), (b) June-August
1146 (JJA), (c) September-November (SON), and (d) December- February (DJF) from 2001 to 2010.
1147 White lines show several major rivers in China.

1152
1153
1154
1155

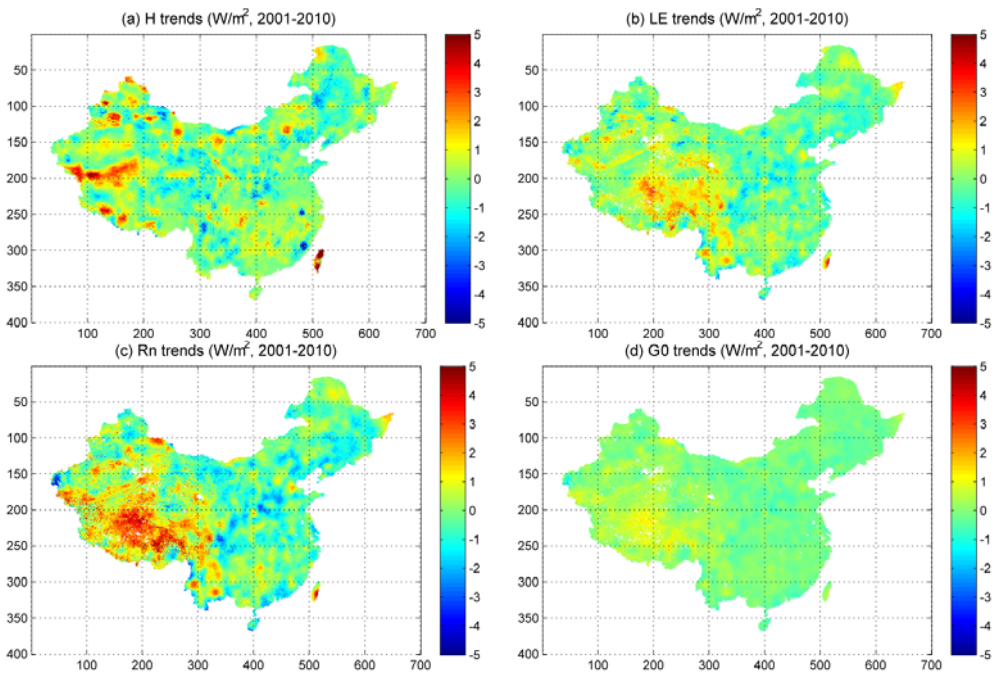


1156
1157

1158 | Figure 129. Spatial trends of (a) SWD (downward short-wave), (b) LWD (downward long-wave),
1159 (c) SWU (upward short-wave), and (d) LWU (upward long-wave radiation) for the Chinese
1160 landmass from 2001 to 2010.

1161
1162
1163
1164
1165
1166

1167
1168
1169
1170



1171
1172

1173 | Figure 130. Spatial trends of (a) sensible heat flux (H), (b) latent heat flux (LE), (c) net radiation
1174 (Rn), and (d) ground heat flux (G0) on the Chinese landmass from 2001 to 2010.

Page 17: [1] Formatted	Chen, X. (ITC)	9/5/2014 9:35:00 AM
------------------------	----------------	---------------------

Font: Times New Roman, 12 pt

Page 17: [2] Formatted	Chen, X. (ITC)	9/5/2014 9:35:00 AM
------------------------	----------------	---------------------

Font: Times New Roman, 12 pt

Page 17: [3] Formatted	Chen, X. (ITC)	9/5/2014 9:35:00 AM
------------------------	----------------	---------------------

Font: Times New Roman, 12 pt

Page 17: [4] Formatted	Chen, X. (ITC)	9/5/2014 9:35:00 AM
------------------------	----------------	---------------------

Font: Times New Roman, 12 pt

Page 17: [5] Formatted	Chen, X. (ITC)	9/5/2014 9:35:00 AM
------------------------	----------------	---------------------

Font: Times New Roman, 12 pt

Page 17: [6] Formatted	Chen, X. (ITC)	9/5/2014 9:35:00 AM
------------------------	----------------	---------------------

Font: Times New Roman, 12 pt

Page 17: [7] Formatted	Chen, X. (ITC)	9/5/2014 9:35:00 AM
------------------------	----------------	---------------------

Font: Times New Roman, 12 pt, Bold